

Toward Sustainable Groundwater Management: Harnessing Remote Sensing and Climate Data to Estimate Field-Scale Groundwater Pumping and Irrigation Efficiencies

Thomas J. Ott ^{a*}, Sayantan Majumdar ^{a*}, Justin L. Huntington ^{a†}, Christopher Pearson ^a,
Matt Bromley ^a, Blake A. Minor ^a, Charles G. Morton ^a, Sachiko Sueki ^b, Jordan P. Beamer ^c,
Richard Jasoni ^a

^a Desert Research Institute, Reno, NV, USA

^b Desert Research Institute, Las Vegas, NV, USA

^c Oregon Water Resources Department, Salem, OR, USA

Abstract

Groundwater overdraft in western U.S. states is resulting in the development of groundwater management plans, which include mandatory reporting of groundwater pumping (*GP*) to track water use. Most basins do not have the infrastructure (flow meters) to monitor *GP*. Of those that do, performing quality assurance and quality control (QAQC) of the reported *GP* data is difficult due to the lack of reliable secondary *GP* estimates. We hypothesize that satellite (Landsat)-based actual evapotranspiration (ET) estimates from OpenET can be used to predict *GP* and aid in QAQC of the reported *GP* data. For this purpose, the objectives of this study are as follows: first, to pair OpenET estimates of consumptive groundwater use (*Net ET*, i.e., actual ET less effective precipitation) and metered annual *GP* data from Diamond Valley (DV), Nevada, and Harney Basin (HB), Oregon; second, to evaluate linear regression and ensemble machine learning (ML) models (e.g., Random Forests) to establish the *GP* vs *Net ET* relationship, and third, to compare *GP* estimates at the field- and basin-

* These two authors have contributed equally.

† Corresponding author at: Division of Hydrologic Sciences, Desert Research Institute, 2215 Raggio Parkway, Reno, Nevada 89512-1095, USA
Email address: justin.huntington@dri.edu (J.L. Huntington)

scales. Using bootstrapping, mean absolute errors (MAEs) for field-scale *GP* depth are 12% and 11% for DV and HB, respectively, and the corresponding root mean square errors (RMSEs) are 15% and 14%. Moreover, the regression models can explain 50%-60% variance in *GP* depth and ~90% variance in *GP* volumes. The estimated average irrigation efficiency of 88% (92% and 83% for DV and HB, respectively) aligns with known center pivot system efficiencies. Additionally, OpenET proves to be useful for identifying discrepancies in the metered *GP* data, which are subsequently removed prior to model fitting. Results from this study illustrate the usefulness of satellite-based ET estimates for estimating GP, QAQC reported *GP* data and has the potential to estimate historical *GP*.

Keywords: groundwater pumping; remote sensing; evapotranspiration; irrigation; machine learning; water use

1. INTRODUCTION

1.1 Background

In the western United States (U.S.), the combination of increased and projected droughts (Meza et al., 2020), rising irrigation water demands, and population growth is expected to intensify groundwater consumption (Huntington et al., 2015), leading to adverse consequences like aquifer depletion (ADWR, 2018; Scanlon et al., 2012; Smith et al., 2017, 2023), land subsidence (Hasan et al., 2023; Herrera-García et al., 2021; Smith & Li, 2021; Smith & Majumdar, 2020), and water contamination (Levy et al., 2021; Smith et al., 2018). Despite these pressing challenges, many groundwater basins in this region lack comprehensive monitoring of groundwater pumping (*GP*). Accurately assessing *GP* is imperative for implementing sustainable strategies to confront water security challenges. Consequently, the development of reliable and efficient solutions for *GP* monitoring holds paramount importance in effectively addressing water management issues in this region.

New water management policies across the western U.S. states have begun to include mandatory reporting of *GP*. These new policies are being sparked by groundwater overdrafts in regions heavily dependent on groundwater. Understanding how much water is being withdrawn from aquifers allows water managers to manage groundwater resources more effectively. Most GP in U.S. western states is used for irrigated agriculture, e.g., in Nevada, California, and Oregon, about 70% to 90% of groundwater is used for irrigation (Dieter et al., 2018). Of the 256 designated hydrologic basins in Nevada, 96 are considered over-appropriated, and in some cases, by more than 300% (NDWR, 2021). Many of these over-appropriated basins are also pumping groundwater at rates above their perennial yield, causing groundwater levels to decline. Other western U.S. states are also experiencing over-appropriation and over-drafting in many of their hydrologic basins (Reilly et al., 2008; Zektser et al., 2005). In response, these regions are actively creating new groundwater management policies and laws to monitor *GP* further (Megdal et al., 2015). Examples of these new policies include the Sustainable Groundwater Management Act in California (SGMA), which seeks to balance basin water budgets (Owen et al., 2019), the Local Enhanced Management Areas (LEMA), which aims to develop enforceable and monitored water use reduction in Kansas (Butler et al., 2018), Active Management Areas (AMAs) and Irrigation Non-Expansion Areas (INAs) in Arizona (ADWR, 2023), and Critical Management Area (CMA) orders and other designations which strive to meter and report all non-domestic GP in dozens of groundwater basins in Nevada (<http://water.nv.gov/StateEngineersOrdersList.aspx>). As the business saying goes, “You can’t manage what you don’t measure.” This axiom is equally true for water resources. Recognizing this fact, developing programs for monitoring and reporting water use to state and local agencies is becoming a common trend with respect to water policy and regulation in the western U.S. (Deines et al., 2019; Megdal et al., 2015).

While metering all *GP* sounds like a simple solution for monitoring and reporting groundwater use, installing meters at all well heads or diversions is a costly process. Additionally, meter readings do not equate to the consumptive use of groundwater, which is the quantity ultimately needed for groundwater management. Perhaps more importantly, *GP* meter data have high uncertainty and are often erroneous (Fanning et al., 2001). Primary sources of uncertainty and error are due to the following variables: a large variation in the quality of meter type, poor meter installation, lack of meter calibration, unnoticed meter drift, meter failure or partial failure, erroneous recording of meter data, meter data input errors such as those commonly associated with self-reporting (Carroll et al., 2010; Little et al., 2016; Sheppard & Terveen, 2011), and lack of quality assurance and quality control (QAQC) procedures and guidelines. In addition, regarding the self-reporting aspect, the validity of the data could be compromised due to the potential of water users acting in bad faith. With large amounts of data being collected and reported either through online self-reporting systems or by state and local agency field surveys, coupled with high uncertainty and potential for errors, questions and concerns around the quality and validity of meter data will likely be a source of conflict for groundwater management in the future. Given these factors, it is important to have complementary, independent, and cost-effective approaches to data collection, which allow for direct *GP* estimates to be obtained, as well as the ability to assess *GP* when no records exist.

1.2 Previous Work

Numerous approaches have been developed for estimating *GP* and consumptive use. Here, we provide a brief overview of some of the more common as well as recently developed approaches.

In the past, electrical power records were one of the most common approaches for estimating *GP* and have been used by many studies (Burt et al., 1997; Frenzel, 1985; Said et al., 2005). This method requires information on pump efficiency, water lift height, and operating pressures (Frenzel, 1985). Error in these factors and their change through time leads to errors in *GP* estimates (Hurr & Litke, 1989). Obtaining power records for well pumps is difficult, especially for rural communities. The use of power records for assessing and estimating *GP* for the purpose of groundwater management is not feasible at large scales.

Current methods for estimating groundwater withdrawals commonly include surveying and organizing county-scale annual water use (Dieter et al., 2018; Martin et al., 2023), process-based models (ADWR, 2018; Ahamed et al., 2022; Brookfield et al., 2023; Dogrul et al., 2016; Faunt, 2009; Ruess et al., 2023) and the recent integrated remote sensing and machine learning-driven approaches (Majumdar et al., 2020, 2021, 2022). County-level estimates offer a comprehensive overview of water usage on a nationwide scale within the conterminous U.S. (CONUS), yet finer spatial or temporal details are lacking (Dieter et al., 2018; Martin et al., 2023).

Process-based models have shown success in specific regions; however, they often cannot effectively utilize the numerous remote sensing datasets accessible, such as field-scale evapotranspiration data— an obvious indicator of *GP* in areas with little to no surface water for irrigation (Bos et al., 2009; Melton et al., 2021). Also, process-based models are computationally intensive and require strict model calibration procedures. The Central Valley Hydrologic Model (CVHM) is one such example of a well-established hydrologic model developed by Faunt (2009), which adopts the MODFLOW FMP package (Schmid, 2004) for simulating water requirements. CVHM integrates land use, surface water supply, and water demand information using an ET model that factors in temperature, crop type, precipitation, and root depth. Following this, CVHM allocates the remaining water demand to *GP*.

Another method involves building lookup tables based on land use derived from remote sensing, modeled precipitation, and in-situ pumping data (Wilson, 2021). However, this approach overlooks the intricate interplays between climate, evaporative demand, land use, and soil composition. Machine learning-based solutions have the capacity to integrate a diverse range of datasets, including remote sensing data and model-generated datasets. Furthermore, these solutions can handle complex relationships among input datasets and have been proven to provide reliable estimates (Filippelli et al., 2022; Lamb et al., 2021; Majumdar et al., 2020, 2021, 2022; Wei et al., 2022).

For data-driven or machine learning-based methodologies, large amounts of quality data are required (Majumdar et al., 2022). Employing machine learning to estimate *GP* requires in-situ pumping measurements on expansive spatial and temporal scales (2002-2020), facilitating the validation of withdrawal quantities across extensive regions. As a result, generating and validating gridded annual *GP* estimates in Kansas (Majumdar et al., 2020) and Arizona (Majumdar et al., 2022) were feasible at 5 km and 2 km spatial resolutions, respectively.

However, *GP* from most aquifers is not measured; instead, only a small proportion of wells are metered (Foster et al., 2020). Additionally, in these areas, groundwater use is monitored to such a limited extent that validation of previously reported water use is often absent. In cases where validation is undertaken, skill metrics are comparatively lower than those of regional groundwater models (Wilson, 2021). Consequently, generating and validating gridded prediction rasters in regions with sparse in-situ *GP* measurements poses a challenge, underscoring the need for a thorough evaluation of model efficacy using cross-validation techniques (Hastie et al., 2001). Furthermore, in regions characterized by sparse datasets—a common scenario in the groundwater domain—cross-validating the total *GP* for each individual pixel, as carried out in data-rich regions like Kansas and Arizona, is not

practicable. Instead, the cross-validation process must be conducted at the scale of individual fields with existing field boundaries, predictor attributes, and meter data.

In addition to these process-based and data-driven methods, there are deterministic approaches to estimating *GP*, which incorporate consumptive groundwater use (water transpired by the crop plus water evaporated from the soil surface) and net irrigation water requirement (NIWR) (water delivered to a system to meet irrigation requirement) (Allen & Robison, 2007; Bos et al., 2009; Huntington & Allen, 2009). These methods are based on reference ET and the single or dual crop coefficient approach (Allen et al., 1998).

Huntington and Allen (2009) used the dual crop coefficient method to estimate consumptive use and NIWR across basins in Nevada. The Nevada Department of Water Resources (NDWR) uses these numbers to estimate *GP* where meter data is absent (NDWR, 2022). The *GP* estimates are calculated by dividing NIWR by the irrigation efficiency factor (0.85 for pivot, 0.75 for wheel lines, and 0.60 for flood irrigation, Howell (2002)) and multiplying by the crop acreage. This approach has been used in many groundwater modeling and water budget studies throughout the western U.S. (Carroll et al., 2010; Huntington et al., 2022; Mefford & Prairie, 2022; NDWR, 1985; OWRD, 2015), and assumes the crop is well-watered, stress-free, and uniformly irrigated, which rarely occurs in all irrigated fields across a basin. Crop conditions and water use are highly variable in time and space due to the following factors: water availability, fallowing, partial irrigation, variation in soil type, crop stress, disease, and diverse farming practices. NIWR or similar potential ET-based approaches do not account for spatial variability in crop conditions but serve as an upper bound for estimating water use. Remote sensing of actual ET addresses many of these shortcomings through field-scale observations of actual field conditions.

1.3 Research Goals and Objectives

While the studies above are the first for estimating gridded (regional- or basin-scale) *GP* using remote sensing and data-driven or process-based approaches, they are not suitable for field-scale applications over large areas and periods. Moreover, field-scale *GP* volumes reported by Filippelli et al. (2022) in parts of the central Ogallala aquifer impose artificial correlations between irrigated fields and *GP* volumes (i.e., a larger field will have higher *GP* than a smaller one). Filippelli et al. (2022)'s study integrating remote sensing and machine learning techniques to estimate field-scale *GP* is also conducted in a data-rich setting (e.g., western Kansas has more than 90% metering, Foster et al. (2020)) like Majumdar et al. (2020, 2021, 2022). Hence, cross-validating the results and testing the spatial and temporal model generalizability with leave-one-area-out and leave-one-year-out strategies (these are based on leave-one-out cross-validation, Hastie et al. (2001); Pedregosa et al. (2011)) are not practicable for data-scarce regions in the western U.S, where *GP* metering programs have recently begun (e.g., 2018 in Nevada and 2016 in Oregon).

At the time of this manuscript preparation, no study has been conducted comparing field-scale satellite-based ET estimates to *GP* depths over many fields and for multiple years and concurrently providing insights into irrigation efficiencies (Howell, 2002). The goal of this study was to conduct such a comparison by developing a regression model between the consumptive groundwater use or *Net ET* (actual ET less effective precipitation) and *GP* depth, which can be used to support QAQC of *GP* records and provide a means to estimate *GP* where meter data is unavailable. This regression will be derived using *GP* data from Diamond Valley (DV), Nevada, and Harney Basin (HB), Oregon, locations where good-quality *GP* data is available. Furthermore, we assess whether machine learning can improve the estimates obtained using linear regression and discuss the importance of developing carefully attributed irrigation data (digitized field boundaries and irrigation water source).

We hypothesize that 1) field-scale satellite-based ET estimates will be well-correlated with field-scale metered *GP* data, and 2) statistical relationships between field-scale satellite-based ET and *GP* data will be useful for QAQC of *GP* records and assessment of prior estimates, and 3) ET-based predictions of *GP* will compare reasonably well to metered *GP* at the field and basin scales. To test these hypotheses, this study 1) employs the OpenET ensemble model to obtain field-scale actual ET, 2) links *GP* and ET values by delineating place of use field boundaries, pairing *GP* with field boundaries, and pairing modeled ET with field boundaries 3) compares *Net ET* estimates with metered *GP* to identify potential outliers, 4) develops a regression model (*GP* as a function of *Net ET*), assesses uncertainty using bootstrapping, and calculates the confidence and prediction intervals for the model, 5) compares predicted *GP* from the regression model with basin totals reported by NDWR and OWRD, 6) evaluates multiple machine learning model performance, and 7) compares the OpenET ensemble with the individual satellite-based ET models.

2. STUDY AREAS AND DATASETS

2.1 Study Areas

In this research, we focus on two study areas: Diamond Valley, Nevada, and Harney Basin, Oregon. DV is located in Central Nevada and is one of the only fully metered groundwater-dependent basins in Nevada and possibly the western U.S. In 2015, the Nevada State Engineer's Office designated the basin as a Critical Management Area, which

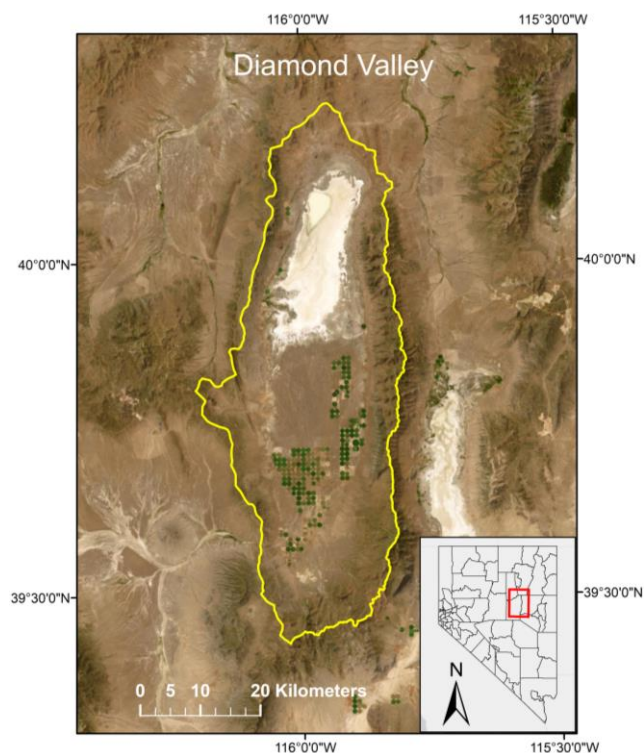


Figure 1. Satellite image of Diamond Valley (DV), Nevada showing the irrigated fields.

initiated the formation of a groundwater management plan (GMP). The plan involved all participating growers installing flow meters selected from the “Idaho Department of Water Resources List of Approved Closed Conduit Flow Meters” and reporting *GP* to the State of Nevada (Bugenig, 2017). The goal of the plan was to reduce *GP* by 55% within the next 35 years. The GMP was implemented in 2018 and continued into 2019, providing *GP* data for those two years, but in May 2020, the plan was struck down by Nevada Courts. However, the state engineer’s order to report *GP* is still active.

DV contains 10,500 hectares (26,000 acres) of irrigated agricultural land, and the estimated *GP* is 94 Mm³/year (76,000 acre-ft/year) (Bugenig, 2017). The estimated groundwater recharge rate is 43 Mm³/year (35,000 acre-ft/year) (Berger et al., 2016), causing groundwater levels to decline, with some areas experiencing nearly 25 m (80 ft) of decline over the last 50 years (Berger et al., 2016). The 30-year average precipitation in the valley is 230 mm/year, with approximately 60% occurring in the winter months. Warmest temperatures occur in July with an average high of 31°C and lowest temperatures in December with an average low of -12°C. The main agricultural crop is alfalfa or other grass hays primarily irrigated with center pivot systems.

Harney Basin is located in south-eastern Oregon, where irrigation is the primary user of groundwater, accounting for 95% of all groundwater use (Beamer & Hoskinson, 2021; Gingerich, Garcia, et al., 2022; Gingerich, Johnson, et al., 2022).

The basin is semiarid in climate and

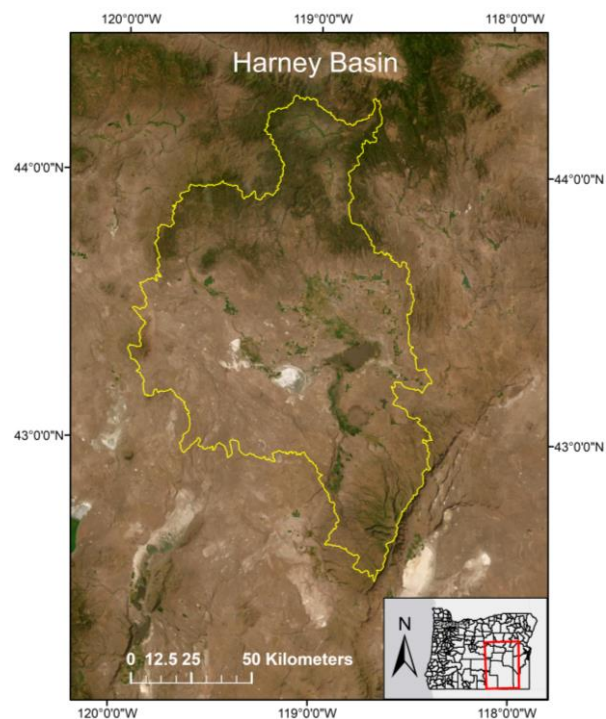


Figure 2. Satellite image of Harney Basin (HB), Oregon showing the irrigated fields.

receives an average of 230 mm to 300 mm of precipitation per year, with most occurring (80%) in the winter months (Beamer & Hoskinson, 2021).

Declining groundwater levels in recent years, likely caused by over-appropriation, have sparked concerns over the sustainability of the resource in HB. Currently, 38,777 hectares (95,821 acres) of permitted primary or supplementary groundwater rights exist in the Greater Harney Valley Area (GHVA) (Beamer & Hoskinson, 2021). The water rights for these permits exceed the estimated recharge for the basin, which is poorly defined. In 2016, the Oregon Water Resources Department (OWRD) co-developed a groundwater study plan with the U.S. Geological Survey (USGS) to facilitate an improved understanding of the groundwater resources and flow systems in HB (Garcia et al., 2021; Gingerich, Johnson, et al., 2022).

The primary crops irrigated in the HB region are alfalfa and grass hay, with May to September being the typical growing season. Additionally, limited quantities of spring and winter grains and mint are also produced in HB (Beamer & Hoskinson, 2021). The irrigation *GP* has nearly tripled during 1991–2018, increasing from about 62 Mm³/year to 185 Mm³/year, i.e., 51,000 acre-ft/year to 150,000 acre-ft/year (Gingerich, Garcia, et al., 2022). Thus, it is essential to develop efficient and reliable field-scale *GP* estimation methods to support the GMPs in both DV, Nevada, and HB, Oregon.

2.2 Datasets

The key datasets in our study include Landsat actual evapotranspiration (ET) from OpenET (Melton et al., 2021), precipitation, and reference ET (ET_o) from gridMET (Abatzoglou, 2013) and the irrigation data comprising of digitized field boundaries and irrigation water source (Huntington et al., 2018; Beamer & Hoskinson, 2021).

2.2.1 *OpenET*

OpenET provides actual ET measurements using data derived from various satellite-driven ET models while also computing a unified "ensemble value" derived from these models. The OpenET ensemble incorporates models that have been utilized by governmental bodies responsible for water use monitoring and management across the Western U.S. Some of these models are also widely adopted on an international scale. These models uniformly utilize Landsat satellite data to generate ET information at a spatial resolution of 30 m. Additional input factors include gridded meteorological variables such as solar radiation, air temperature, humidity, wind speed, and, in certain instances, precipitation data (Melton et al., 2021). Table 1 shows the current ET models used for generating the OpenET ensemble. Most of these models are developed using either complete or simplified adaptations of the surface energy balance (SEB) methodology.

The SEB approach effectively factors in the energy required to convert liquid water within plants and soil into vapor, which is subsequently released into the atmosphere (Laipelt et al., 2021). For both the daily and monthly OpenET ensembles, Melton et al. (2021) observed a strong correlation with the flux tower ET, low overall bias errors, and combined error metrics, i.e., root mean square error (RMSE) and mean absolute error (MAE), lying within 13–30 mm/month and 0.7–1.4 mm/day. With actual ET measurements at the field scale, the OpenET ensemble product is the most important input dataset in our study.

288 **Table 1.** Existing ET models in the OpenET ensemble [reproduced from OpenET (2023)].

Model Acronym	Model Name	References
ALEXI/DisALEXI v 0.0.32	Atmosphere-Land Exchange Inverse / Disaggregation of the Atmosphere- Land Exchange Inverse	Anderson et al. (2007, 2018)
eeMETRIC v 0.20.26	Google Earth Engine implementation of the Mapping Evapotranspiration at high Resolution with Internalized Calibration model	Allen et al. (2005, 2007, 2011)
geeSEBAL v 0.2.2	Google Earth Engine implementation of the SEB Algorithm for Land	Bastiaanssen et al. (1998); Laipelt et al. (2021)
PT-JPL v 0.2.1	Priestley- Taylor Jet Propulsion Laboratory	Fisher et al. (2008)
SIMS v 0.1.0	Satellite Irrigation Management Support	Melton et al. (2012); Pereira et al. (2020)
SSEBop v 0.2.6	Operational Simplified SEB	Senay (2018); Senay et al. (2013, 2022)

289 **2.2.2 gridMET**

290 The gridMET dataset (Abatzoglou, 2013) offers a comprehensive collection of daily surface
291 measurements, including temperature, precipitation, winds, humidity, and radiation across the
292 CONUS from 1979 at ~4 km spatial resolution. This dataset integrates the openly available
293 ~4 km spatial data from the Parameter-elevation Relationships on Independent Slopes Model

(PRISM) (Daly et al., 2008) with the high temporal-resolution data from the National Land Data Assimilation System (NLDAS) (Xia et al., 2012). The validation metrics over the western U.S. indicate favorable results, with $\pm 5\%$ precipitation bias. Gridded daily grass reference ET (ET_o) also displayed a strong correlation to daily ET_o measurements (median Pearson's correlation coefficient of 0.9), although it displayed a positive bias across most sites (median bias +0.5 mm). Since the gridMET product is operationally used in OpenET (Melton et al., 2021), we rely on the gridMET ET_o and precipitation data to calculate the effective precipitation and consumptive groundwater use, i.e., *Net ET*.

2.2.3 Irrigation Data

Irrigation data comprising carefully attributed irrigated field boundaries and water source type are critical for field-scale *GP* estimation. Here, we describe these datasets and their importance in performing field-scale assessments of *GP* and ET.

2.2.3.1 Digitized irrigation field boundaries

The field boundaries for each study year were derived from the U.S. Department of Agriculture (USDA) Common Land Unit (CLU) data representing the acreage in 2008 (USDA Farm Service Agency, 2017). These boundaries were manually adjusted using visualizations of high-resolution National Agricultural Imagery Program (NAIP) data (USDA, 2023) and mapped water rights obtained from state water agencies. In years without NAIP data, Landsat false color composites for the specific year were employed, along with NAIP and National Land Cover Database (NLCD) data (<https://www.mrlc.gov/>) from nearby years, to create a comprehensive annual field boundary dataset (Beamer & Hoskinson, 2021; Huntington et al., 2018).

Changes in field boundaries were primarily observed when fields traditionally irrigated with flood or sprinkler-line systems were transformed into center-pivot irrigation or when new

fields were brought into production. Figure 3 illustrates examples of mapped field boundaries in the central GHVA portion of the HB for 1991 and 2016. Each year, the individual polygons representing field boundaries were assigned a unique ID along with the start year of active irrigation, signifying the year when the field was initially identified in the imagery as actively irrigated (Beamer & Hoskinson, 2021).

These carefully attributed and digitized irrigation field boundaries are used in the OpenET individual models as well as the ensemble product to generate field-scale actual ET estimates throughout the western U.S. (Melton et al., 2021).

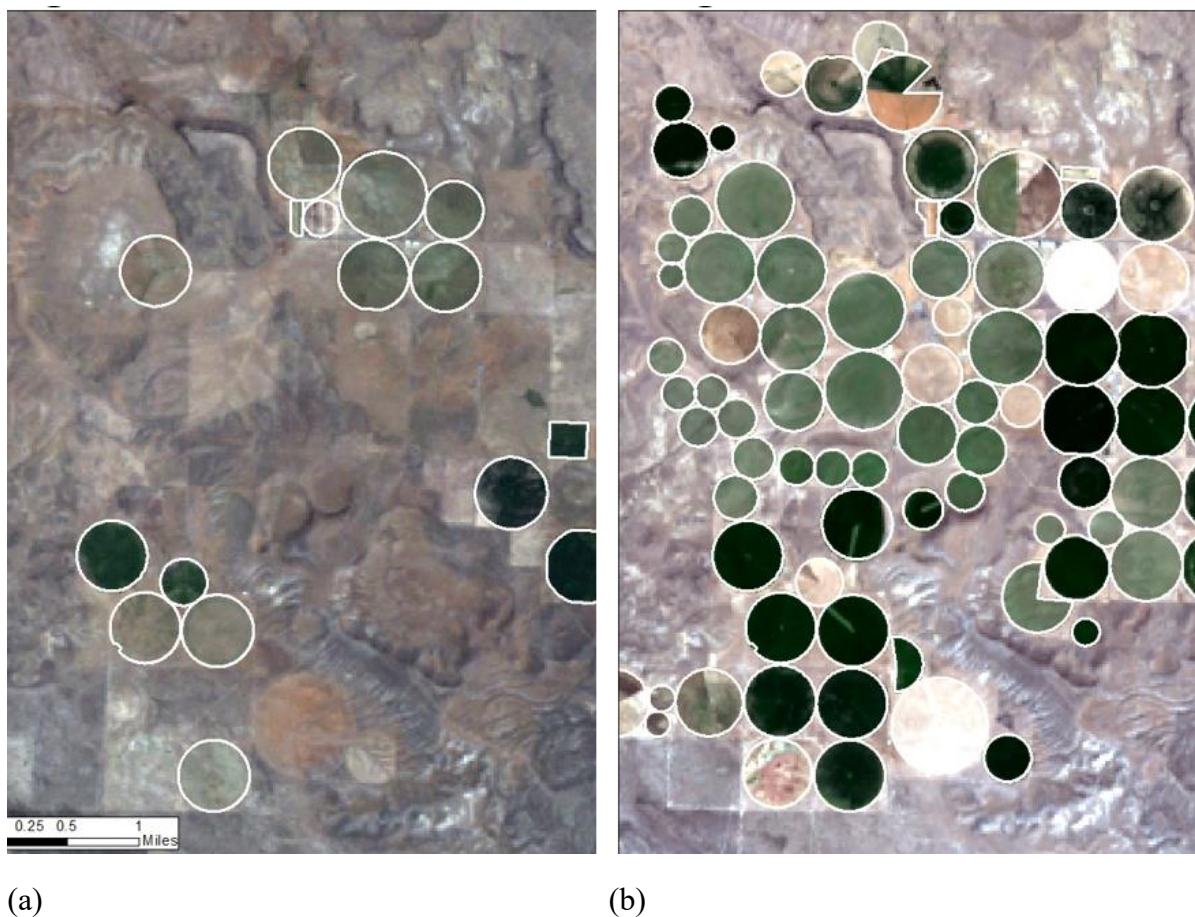


Figure 3. Digitized irrigated field boundaries in the GHVA portion of HB, Oregon (reproduced from Beamer and Hoskinson (2021)). The massive increase in irrigation and changes from square fields to circles between (a) August 1991 and (b) August 2016 showcases the need for maintaining and updating our irrigation field boundary dataset. The field boundary shape changes are due to switching irrigation systems, i.e., from flood or sprinkler-line systems to center pivots.

2.2.3.2 Water source type

While DV, Nevada irrigation is entirely groundwater dependent (NDWR, 2020), HB, Oregon relies on groundwater, surface water, or a combination of these two for irrigation (Beamer & Hoskinson, 2021; Garcia et al., 2021). Since the focus of our study is to estimate field-scale irrigation *GP*, having a water source type attribute to the digitized fields is essential to remove fields that are irrigated with surface water and/or a combination of surface water and groundwater.

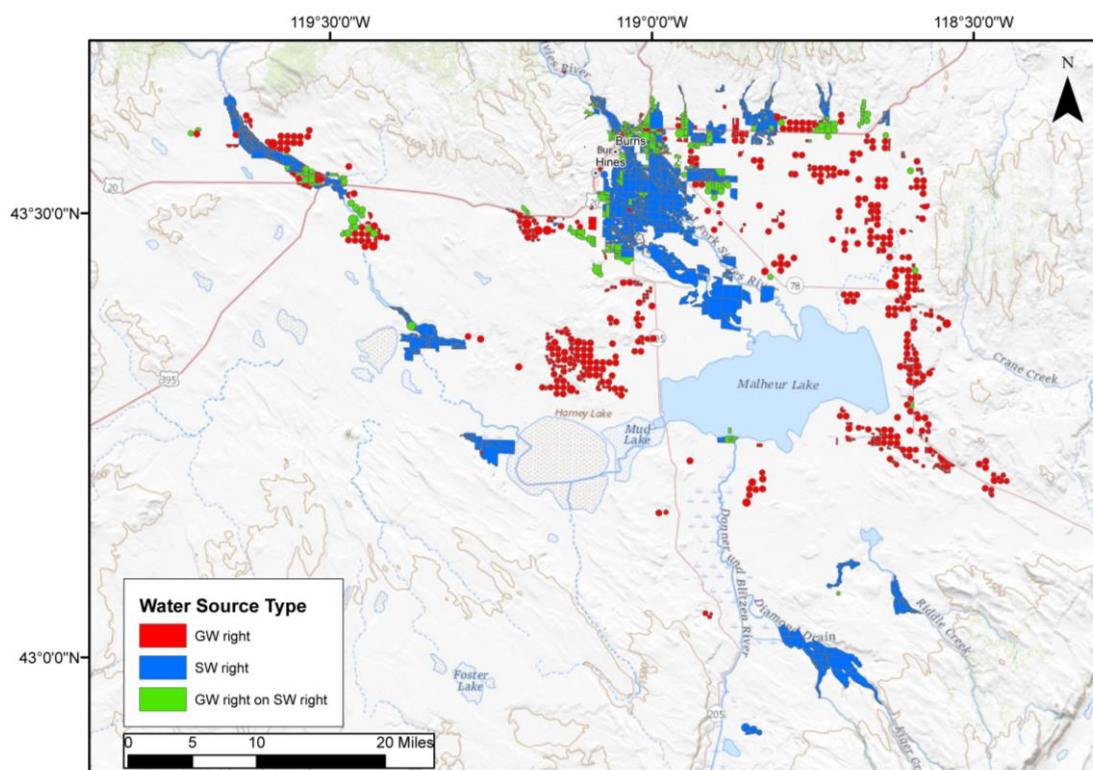


Figure 4. Mapped irrigated field boundaries in the GHVA, HB, Oregon for 2016 with the associated water source type (reproduced from Beamer and Hoskinson (2021)). GW right, SW right, and GW right on SW represent groundwater, surface water, and combination source types, respectively.

The annual field boundaries were associated with specific irrigation source types: groundwater irrigated (GW), surface water irrigated (SW), or a combination of groundwater and surface water (GW&SW). The initial stage in determining the irrigation source type

involved overlaying the annual field boundaries with the OWRD-mapped dataset of water rights place of use (POU). The irrigated POU dataset for the Harney Basin was categorized into areas with exclusively groundwater rights, exclusively surface water rights, and areas with both surface water and groundwater rights where they intersected. For each year, only the POU polygons with priority dates for that year and all preceding years were incorporated into the analysis to depict irrigation development accurately. The chosen POU polygons were then transformed into a 30 m raster using the USGS 3D Elevation Program (3DEP) 30 m Digital Elevation Models (DEMs) (USGS, 2023). Cells within this raster were categorized into irrigation source types using integer values (1 = GW irrigated, 2 = SW irrigated, 3 = Combination). The resultant POU irrigation raster for the year 2016 is illustrated in Figure 4. Beamer and Hoskinson (2021) provide more details on this approach.

2.2.4 Additional Datasets

In addition to the datasets discussed, we rely on several other remote sensing and climate data serving as predictors for the machine learning models (Section 4.3). These datasets are intricately related to the hydrologic and hydroclimatic processes driving *GP*. These include the gridMET (Abatzoglou, 2013) minimum and maximum air temperature, minimum and maximum relative humidity, vapor pressure deficit, grass reference ET, alfalfa reference ET, and wind velocity. Moreover, we use the Daymet v4 precipitation data (~1 km spatial resolution, Thornton et al., 2021), Landsat-8 32-day normalized difference vegetation index (NDVI) composite (30 m, courtesy of the USGS), NASA digital elevation model (NASADEM, 30 m, NASA JPL, 2020), conterminous U.S. (CONUS) 800-m soil properties that include the hydrologic soil group (HSG), soil depth, and the saturated hydraulic conductivity (Walkinshaw et al., 2022), and the OpenET ensemble actual ET as well as the individual model actual ETs (Melton et al., 2021, Table 1).

3. METHODS

3.1 Matching Point of Diversions, Meter Readings, and Places of Use

One of the major challenges in this project is matching the metered *GP* data with the field-scale ET data. Groundwater applications in the State of Nevada are required to include a Point of Diversion (POD) (often a well) and POU, i.e., the maximum area over which water from the POD can be applied (<https://www.leg.state.nv.us/nrs/nrs-533.html>). Multiple applications can be filed for a single well, allowing multiple PODs and POUs for the same area (i.e., stacked water rights).

Reported *GP* values for each well (can be several) are totaled and assigned to the senior most water right by the Nevada State Engineers Office (NSEO). These groups of POUs were joined into a single polygon representing the total area of application. However, since a POU typically extends beyond

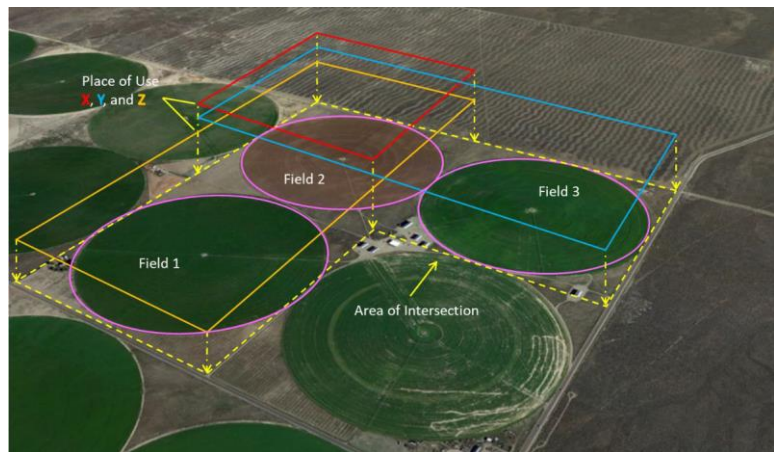


Figure 5. POUs X, Y, and Z paired with the OpenET fields 1, 2, and 3 using spatial intersection in Diamond Valley, Nevada. This is an illustration of a one-to-one mapping with one total pumping value being paired with one OpenET ensemble actual ET estimate. This process is replicated for the Harney Basin, Oregon.

actual irrigated areas (e.g., quarter section POU with center pivot irrigated area within, see Figure 3), we cannot directly use the POU to estimate satellite-based ET. To better define irrigated areas, we relied on Geographic Information System (GIS) and Python software (Van Rossum & Drake, 2009) to spatially join the POU polygons with the irrigated area database (Section 2.2.3) developed by the Desert Research Institute as part of the OpenET project (Huntington et al., 2018; Melton et al., 2021). More specifically, we use Geopandas (Jordahl et al., 2020) to spatially join the grouped POU data from the NSEO and the irrigated area

polygons from OpenET. Figure 3 illustrates this process where POU's X, Y, and Z are grouped with fields 1, 2, and 3. This grouping is "one-to-one," where one total GP value is paired with one Area of Intersection (AoI) ID and, ultimately, one satellite-based ET estimate for the irrigated area. This one-to-one pairing process was replicated for the HB, wherein the OWRD-provided POU groupings were matched to irrigated area polygons from OpenET, like Beamer and Hoskinson (2021).

3.2 Effective Precipitation and Consumptive Groundwater Use

Effective precipitation is the amount of total precipitation on the cropped area that is available to meet the potential ET requirements in that area (Bos et al., 2009). Typically, it is computed by subtracting losses due to runoff and deep percolation beyond the rootzone of the crops from the total precipitation (Allen et al., 1998). Numerous methods exist for estimating effective precipitation, ranging from simple approaches (e.g., a ratio of reference ET and precipitation) to more intricate methods (e.g., involving detailed soil water balance and crop modeling) (Dastane, 1974; Kumar et al., 2017). Many empirical techniques are tailored to specific conditions, and their accuracy and applicability beyond those specific conditions are often limited unless they account for the factors influencing infiltration, runoff, and deep percolation (Feddes et al., 1988; Huntington et al., 2015, 2022; Stamm, 1967; USDA SCS, 1993).

Patwardhan et al. (1990) demonstrated the superior accuracy of the daily soil water balance method in estimating effective precipitation. This method considers soil moisture and plant available water, considering the water-holding capacity and root depths specific to crop areas within each model cell. The runoff from precipitation is computed using the USDA Natural Resources Conservation Service (NRCS) curve number (CN) method (USDA NRCS, 2004).

CN values are scaled between dry and wet conditions based on antecedent soil water content, employing Hawkins et al. (1985)'s expressions.

In this study, we compute the basin-scale effective precipitation fraction (P_{effr}) using the U.S. Bureau of Reclamation (USBR) ET-Demands model (Huntington et al., 2015, 2022; USBR, 2019). This model incorporates various factors, including daily gridMET precipitation data (Abatzoglou, 2013), antecedent soil moisture before a precipitation event, and deep percolation and surface runoff from precipitation. The ET-Demands model utilizes daily weather information, including reference evapotranspiration (ET_o), in conjunction with crop-specific growth curves. Widely applied, it has been used to assess historical and future irrigation water demands for specific USBR irrigation projects (USBR, 2016) and to estimate historical and future irrigation water requirements for the USBR's WaterSMART Basin Studies Program (USBR, 2023). However, we did not compute the effective precipitation directly from ET-Demands because it produces basin-scale outputs. Instead, we used ET-Demands to generate the basin-scale P_{effr} and then computed the field-scale effective precipitation, P_{effld} (more details in Equation 1).

The *Net ET* or consumptive groundwater use is defined in Equation 1 as the actual ET (ET_a) minus effective precipitation (P_{effld}). Here, we must subtract the portion of precipitation that is considered 'effective' or contributes to ET, i.e., P_{effld} , from the total ET_a because it includes ET derived from precipitation (P_{field}). Note that, because our study focuses on estimating *GP* in fully groundwater-dependent irrigation fields, we specifically use the term 'consumptive groundwater use' throughout this manuscript instead of the generic 'consumptive use.' These *Net ET* estimates are foundational not only for estimating *GP* but also for assessing irrigation application rates and irrigation water requirements (Huntington et al., 2022).

$$Net\ ET = ET_a - P_{efield} \quad (1)$$

where,

Net ET: Field-scale consumptive groundwater use.

ET_a: Total annual (January 1 to December 31) field-scale actual ET from the OpenET ensemble product (Melton et al., 2021).

$P_{efield} = P_{efr} * P_{field}$, the field-scale effective precipitation.

P_{efr} : Basin-scale effective precipitation fraction from ET-Demands (USBR, 2019).

P_{field} : Total annual gridMET precipitation (originally at ~4 km spatial resolution, Abatzoglou (2013)) aggregated at the field scale using spatial reductions available through the Google Earth Engine Python API (Gorelick et al., 2017).

3.3 Estimating Field-Scale Groundwater Pumping

We use the least-squares linear regression (Equation 2) to develop individual DV and HB-specific regression models between *GP* depth and *Net ET*. To make the model independent of area, we consider *GP* depths rather than *GP* volumes, i.e., dividing the reported pumping volumes from NDWR and OWRD by the respective irrigated field areas in the associated AoI (Figure 5).

$$GP = \hat{\beta}_0 + \hat{\beta}_1 * Net\ ET + \epsilon \quad (2)$$

where,

GP: Metered annual groundwater pumping depth.

Net ET: Field-scale consumptive groundwater use (Equation 1).

$\hat{\beta}_0, \hat{\beta}_1$: Regression coefficients.

ϵ : Random error associated with estimating *GP*.

Prior to fitting the regression model, we remove fields with *GP/Net ET* ratios lying outside the (0.5, 1.5) interval. We obtain this interval based on histogram analysis (Figure 6 (a)) and

boxplot-derived lower and upper limits (based on the interquartile range, Figure 6 (b), Hastie et al. (2001)) of the $GP/Net\ ET$ ratios for DV, Nevada. Essentially, we remove fields where the reported metered GP data are below 50% or above 150% of the consumptive groundwater use.

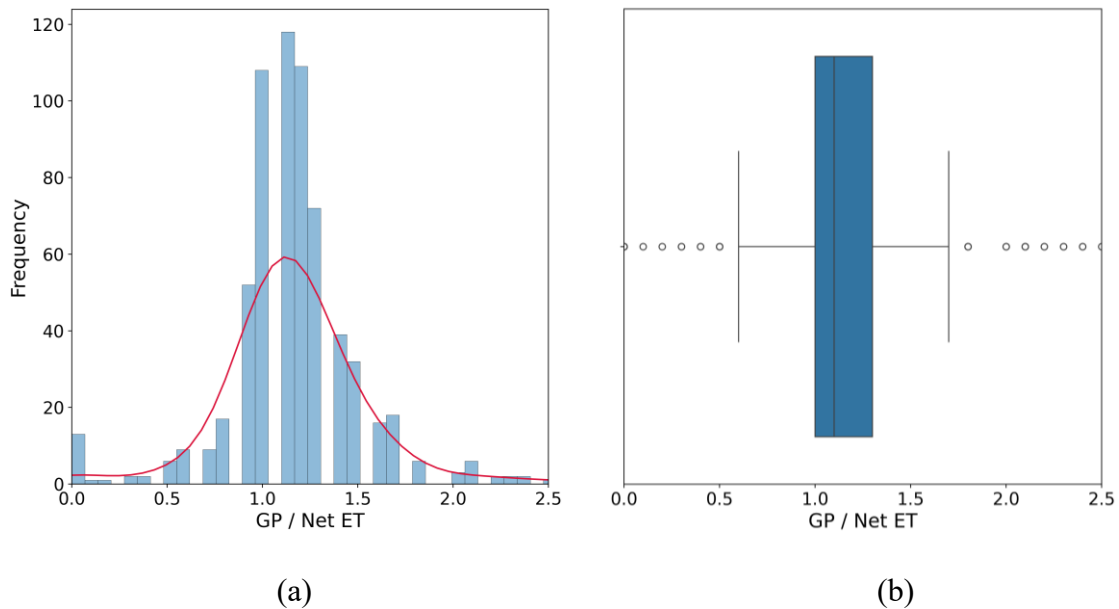


Figure 6. The (a) histogram and (b) boxplot distributions of the GP and $Net\ ET$ ratios over DV, Nevada. The red line in (a) denotes the kernel density estimate (Hastie et al., 2001) of $GP/Net\ ET$, and the x-axis is cutoff at $GP/Net\ ET = 2.5$.

These discrepancies are typically caused due to flowmeter issues and changes in the flowmeters. In addition to applying the same (0.5, 1.5) interval, we remove ten fields in HB, Oregon, with purely surface water rights and combined groundwater and surface water rights based on the water source type data (Figure 4). Furthermore, for both DV and HB, we only consider fields where $GP > 0$. Overall, we discard 19% and 67% of the original DV and HB metered GP data, respectively, which essentially showcases the necessity for relying on field-scale ET to directly estimate GP as developing robust metering infrastructure is not trivial.

As for model evaluation, we employ bootstrapping (Hastie et al., 2001) to estimate the confidence intervals of the regression model. The nonparametric approach of bootstrapping provides a means of estimating confidence intervals and standard errors for the regression

coefficients when relatively little data is available. The least-squares regression provides an estimate of the model parameters, these are not the true values of model parameters since the entire population is unknown and thus would be different if other data were used.

Here, we take a random sample with replacement using all data points, perform the least-squares regression (Equation 2) without fitting the intercept (i.e., $\hat{\beta}_0 = 0$), and estimate the regression coefficient $\hat{\beta}_1$. This process is repeated 1000 times after which we report the coefficient of determination (R^2), RMSE, MAE, and the coefficient of variation (CV, i.e., standard deviation of the predictions divided by the mean of the predictions). Note that we deliberately set $\hat{\beta}_0 = 0$ because, theoretically, GP is the ratio of the *Net ET* and irrigation efficiency (Section 3.1.4) (Howell, 2002).

We then compute the confidence interval (CI) and prediction interval (PI) using the bootstrap percentile interval method, which assigns the lower and upper 95% CI and PI values to the 2.5th and 97.5th percentile of the resulting bootstrap distributions. Moreover, we compare the predicted GP to the actual GP (both depth and volumes) at the field scale, perform basin-scale GP assessments, and analyze the observed GP residuals to test for normality (Sections 4.1 and 4.2). Additionally, we evaluate the performance of the linear regression model against ensemble machine learning algorithms, such as Random Forests (RF) (Breiman, 2001), Gradient Boosting Trees (GBT) (Friedman, 2001), and Extremely Randomized Trees (ERT) (Geurts et al., 2006) available through the scikit-learn (Pedregosa et al., 2011) and LightGBM (Ke et al., 2017) Python APIs (Section 4.3).

3.4 Calculating Irrigation Efficiency

The irrigation efficiency ($IE \in [0,1]$), as defined in Equation 3, is the ratio of the *Net ET* and GP (Howell, 2002). Conversely, GP can be obtained by dividing the *Net ET* by the IE .

Therefore, the inverse of the slope of the fitted regression in Equation 2, i.e., $\hat{\beta}_1^{-1}$, gives us

the IE (since $\hat{\beta}_0 = 0$). Here, we use the terms ‘irrigation efficiency’ and ‘application efficiency’ interchangeably (Howell, 2002).

$$IE = \frac{Net\ ET}{GP} \quad (3)$$

4. RESULTS AND DISCUSSION

4.1 Field-scale GP estimates in DV, Nevada

We observe a good agreement ($R^2 = 0.6$, RMSE = 15.33%, MAE = 12.11%, CV=20.44%) between the metered GP depths and the predicted GP depths at the field scale using linear regression (Equation 2) over DV (Figure 7 (a)).

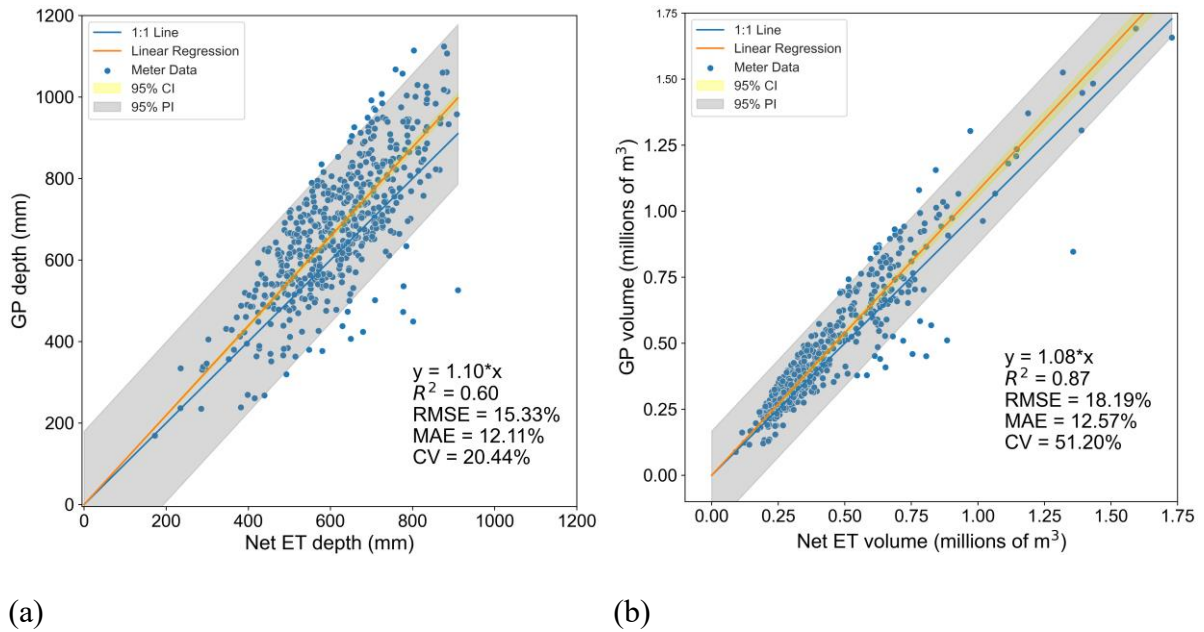


Figure 7. Scatter plots of the fitted (a) GP depth and (b) GP volumes over DV, with the $Net\ ET$ depth and $Net\ ET$ volume as the corresponding predictors. There are a total of 533 samples after the outlier removal process (Section 3.3). The 95% CI and PI are obtained using bootstrapping. Here, y and x denote the response (GP) and the predictor ($Net\ ET$) variables, respectively. The RMSE and MAE percentages are obtained by dividing the RMSE and MAE by the mean of the actual metered GP depth/volume.

Additionally, we achieve $R^2 = 0.87$, RMSE = 18.19%, MAE = 12.57%, and CV = 51.2% when the predicted and metered depths are converted to the volume space by multiplying the irrigated field boundary areas (Figure 7 (b)). This substantial increase in the R^2 can be

attributed to the artificial correlations imposed by multiplying the field areas, i.e., a larger field will have higher *GP* volume than a smaller one, which is also evident from the ~31% increase in the CV (the predicted volumes have a higher variability than the depths because of the varying field areas). Nevertheless, we report the error metrics in both the depth and volume space to demonstrate the effectiveness of our approach.

The slopes of 1.1 and 1.08 in Figures 7 (a)-(b) indicate that the average *IE* for DV is about 92%, which aligns with typical center pivot system efficiencies (Howell, 2002). Accordingly, the standardized *GP* depth residuals, calculated as observed *GP* depth minus predicted *GP* depth, approximately follow a normal distribution (skewness = -0.59, kurtosis = 1.15) and mostly lie in the [-2, 2] interval (Figure 8 (a)). There are also no observable systematic patterns in the standardized *GP* depth residual vs. the *Net ET* depth scatter plot (Figure 8 (b)). Moreover, the basin-scale comparison (Figure 9) of the metered and predicted annual total *GP* volumes further showcases the reliability of our approach.

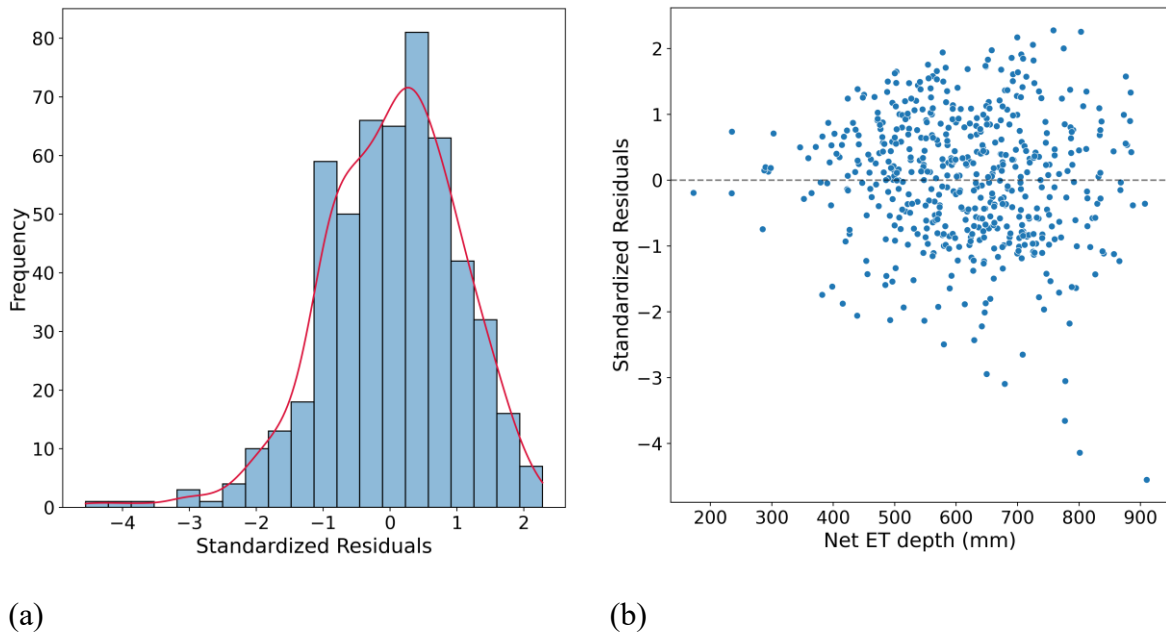


Figure 8. Residual analysis for the fitted linear regression using the DV meter data showing the (a) standardized residual histogram and (b) scatter plot of the standardized residuals vs. *Net ET* depth. The residuals are calculated as observed *GP* depth minus the predicted *GP* depth. The red line in (a) denotes the kernel density estimate like before in Figure 6 (a).

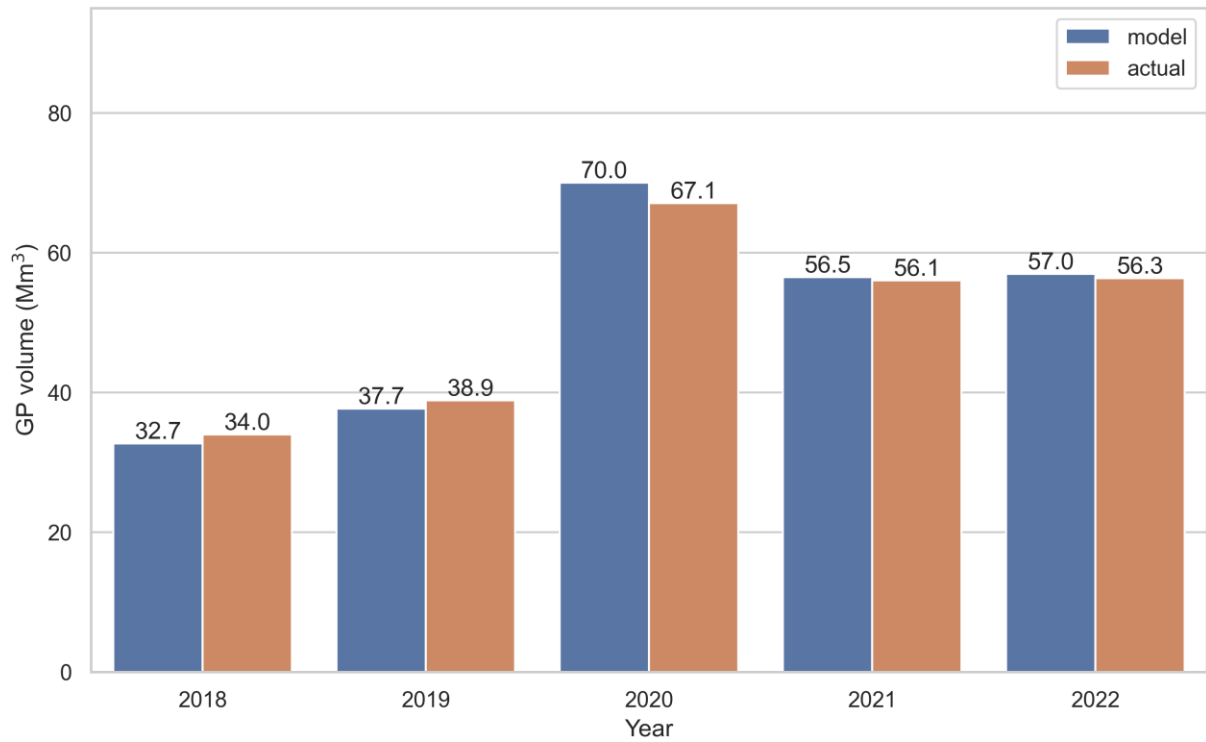


Figure 9. Comparison of the basin-scale total annual *GP* volumes in DV, Nevada. Note that the actual *GP* volumes are computed using the field data which are kept after the outlier removal process (Section 3.3).

4.2 Field-scale *GP* estimates in HB, Oregon

For HB, Oregon, we observe a satisfactory agreement ($R^2 = 0.46$, RMSE = 13.56%, MAE = 11.09%, and CV = 13.41%) between the metered *GP* depths and the predicted *GP* depths at the field scale using linear regression (Figure 10 (a)). Additionally, we obtain $R^2 = 0.88$, RMSE = 13.87%, MAE = 10.8%, and CV = 34.97% considering the *GP* volumes (Figure 10 (b)). These substantial increases in the R^2 and CV are due to the artificial correlations imposed by the field areas, and the variability of the field areas, respectively.

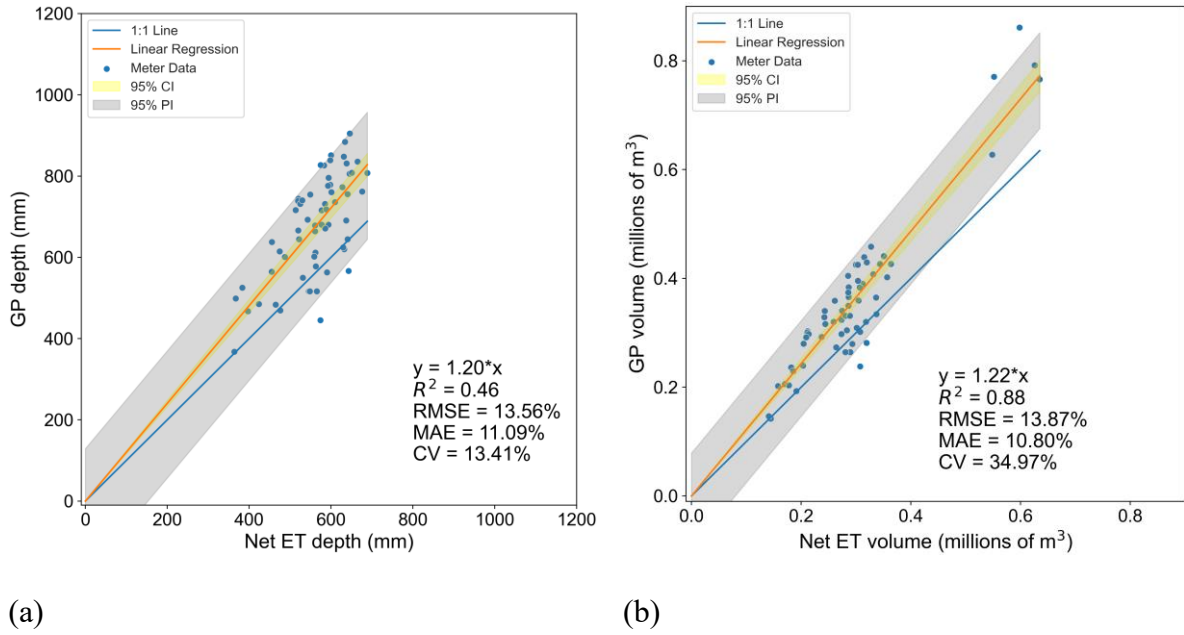


Figure 10. Scatter plots of the fitted (a) *GP* depth and (b) *GP* volumes over HB, with the *Net ET* depth and *Net ET* volume as the corresponding predictors. There are a total of 62 samples after the outlier removal process (Section 3.3).

The slopes of 1.2 and 1.22 in Figures 10 (a)-(b) imply an average *IE* of 83%, which aligns with typical center pivot system efficiencies (Howell, 2002). However, the HB *IE* is about 9% less than that of DV. The standardized *GP* depth residuals approximately follow a normal distribution (skewness = -0.56, kurtosis = -0.39) and mostly lie in the [-2, 1] interval (Figure 11 (a)). Like DV, there are no observable systematic patterns in the standardized *GP* depth residual vs. the *Net ET* depth scatter plot (Figure 11 (b)). Additionally, the basin-scale comparison (Figure 12) of the metered and predicted annual total *GP* volumes shows good agreement and again demonstrates the reliability of our approach.

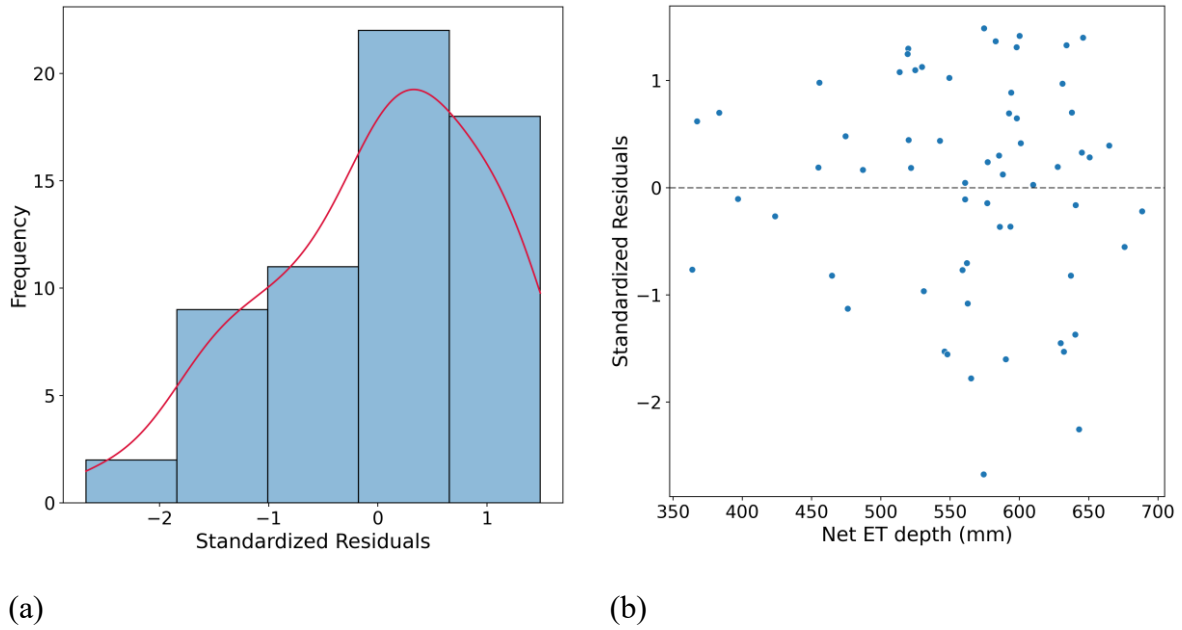


Figure 11. Residual analysis for the fitted linear regression using the HB meter data showing the (a) standardized residual histogram and (b) scatter plot of the standardized residuals vs. *Net ET* depth. The residuals are calculated as observed *GP* depth minus the predicted *GP* depth. The red line in (a) denotes the kernel density estimate like before in Figure 6 (a).

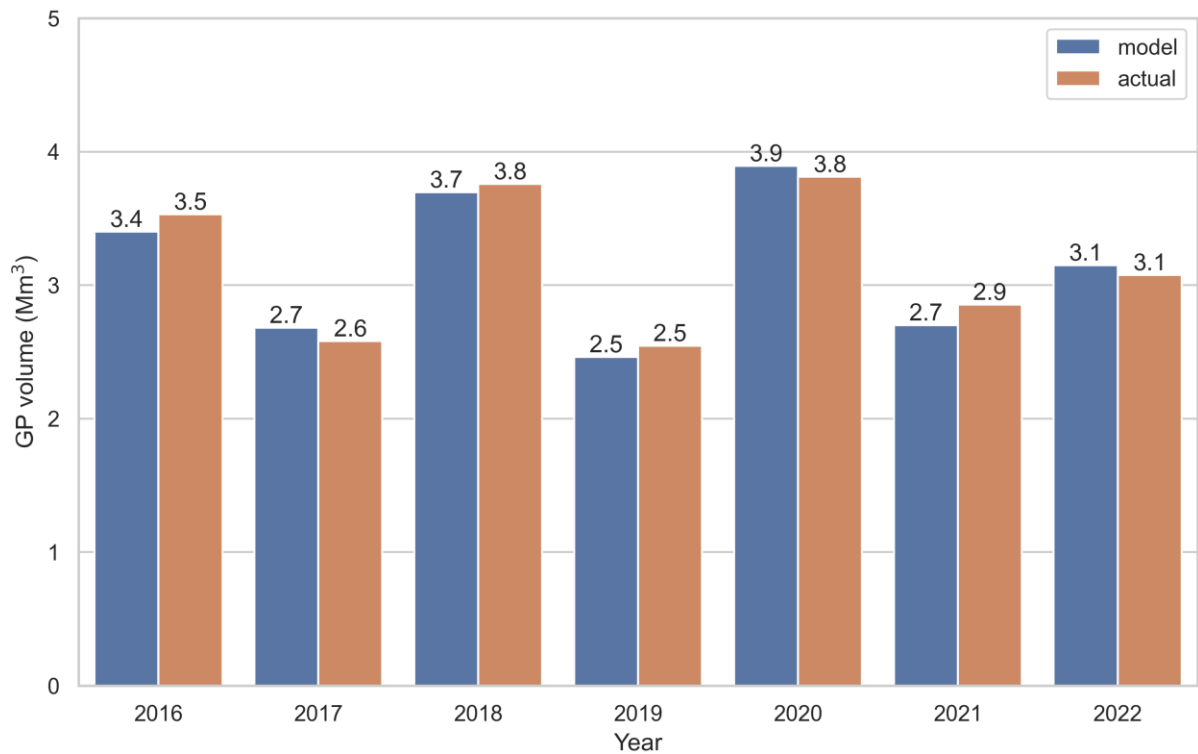


Figure 12. Comparison of the basin-scale total annual *GP* volumes in HB, Oregon. Note that the actual *GP* volumes are computed using the field data which are kept after the outlier removal process (Section 3.3).

4.3 Comparison with Ensemble Machine Learning

Here, we only compare the linear regression and ensemble ML model performances for predicting *GP* depth over DV, Nevada, consisting of 533 valid samples (2018-2022). Since there are only 62 valid samples in HB, Oregon (2016-2022), developing ML models is unreasonable.

Table 2. The training, validation, and test error metrics (rounded to two decimal places) for the ensemble ML models. The ERT model shows the best performance across all metrics for the test data and has the least overfitting, i.e., training, validation, and test error metrics are closer to each other compared to the other models (GBT has the highest overfitting).

Data	Metrics	Ensemble ML models		
		ERT	GBT	RF
Training	R^2	0.73	0.95	0.82
	RMSE (%)	12.21	3.39	10.07
	MAE (%)	9.51	2.54	7.89
	CV (%)	16.61	22.75	19.0
Validation	R^2	0.56	0.53	0.58
	RMSE (%)	15.84	16.42	15.5
	MAE (%)	12.29	12.75	12.12
	CV (%)	15.42	20.29	17.63
Test	R^2	0.63	0.62	0.63
	RMSE (%)	14.82	14.94	14.91
	MAE (%)	11.46	11.68	11.59
	CV (%)	17.43	18.21	17.78

We perform a random 70%-30% training and test data split to assess the model performances through five-fold cross-validation (Hastie et al., 2001). The training, validation, and test metrics are shown in Table 2, where the validation data are automatically generated using the

five-fold cross-validation technique, i.e., 20% of the training data are used to tune the hyperparameters of each ML model (Supplementary Table 1). We use the OpenET ensemble product to calculate *Net ET* like the linear regression model and include all other actual ET models (Table 1) as input predictors along with additional predictors described in Section 2.2.4. Overall, there are 28 predictors in our ML models listed in Supplementary Table 2.

We find that the ERT model gives the best prediction performance with test $R^2 = 0.63$, RMSE = 14.82%, MAE = 11.46%, and CV = 17.43%, which is marginally better than the DV, Nevada linear regression model ($R^2 = 0.6$, RMSE = 15.33%, MAE = 12.11%, and CV = 20.44%, Section 4.1). The corresponding permutation importance (Breiman, 2001) plots of the top five features or predictors for the training and test data are shown in Supplementary Figures 1 and 2, respectively. These show that the *Net ET*, field-scale actual ET, air temperature, relative humidity, soil depth, effective precipitation, and NDVI constitute the key predictors across the three ML models, with *Net ET*, being the most important one as removing it from the predictor set substantially decreases the model performance, with an average 12%-15% increase in training (including validation) RMSE, and 9%-11% increase in test RMSE.

Thus, the linear regression and ensemble ML model results strongly support the three hypotheses of our study (Section 1.3), i.e., 1) field-scale satellite-based ET estimates are well-correlated with field-scale metered *GP* data, 2) statistical relationships between field-scale satellite-based ET and *GP* data are useful for QAQC of *GP* records and assessment of prior estimates, and 3) ET-based predictions of *GP* compare reasonably well to metered *GP* at the field and basin scales.

4.4 OpenET Ensemble vs. Individual ET Models

Here, we compare the performance of the individual OpenET models (Table 1) with that of the OpenET ensemble in predicting *GP* depths using both linear regression (DV and HB) and ML (only DV) methods.

4.4.1 ET comparison through Linear Regression

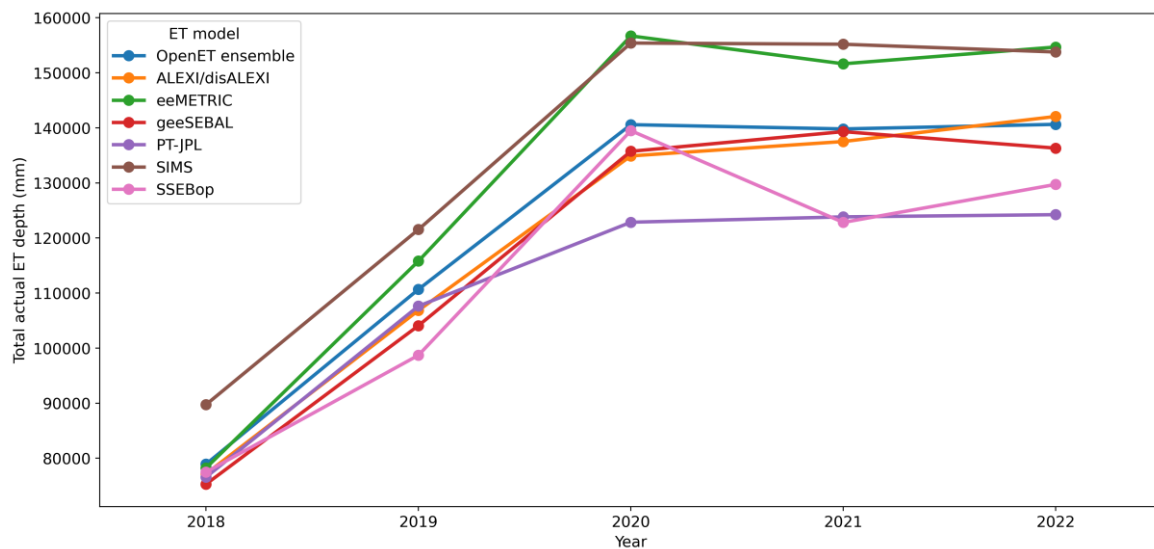
In DV, Nevada, the OpenET ensemble produces the best error metrics in estimating the *GP* depths (Table 3, Figure 7 (a)). For each model (Supplementary Figures 3 (a)-(f)), we use the same (0.5, 1.5) interval for removing the outliers based on the *GP/Net ET* ratios, where the *Net ET* is calculated using the OpenET ensemble and the ET-Demands-derived effective precipitation (Section 3.2).

Table 3. Comparison of the linear regression model metrics (*GP* depths, DV, Nevada) and slopes for different field-scale ET models used to calculate the *Net ET*. The metrics and slopes are rounded to two decimal places.

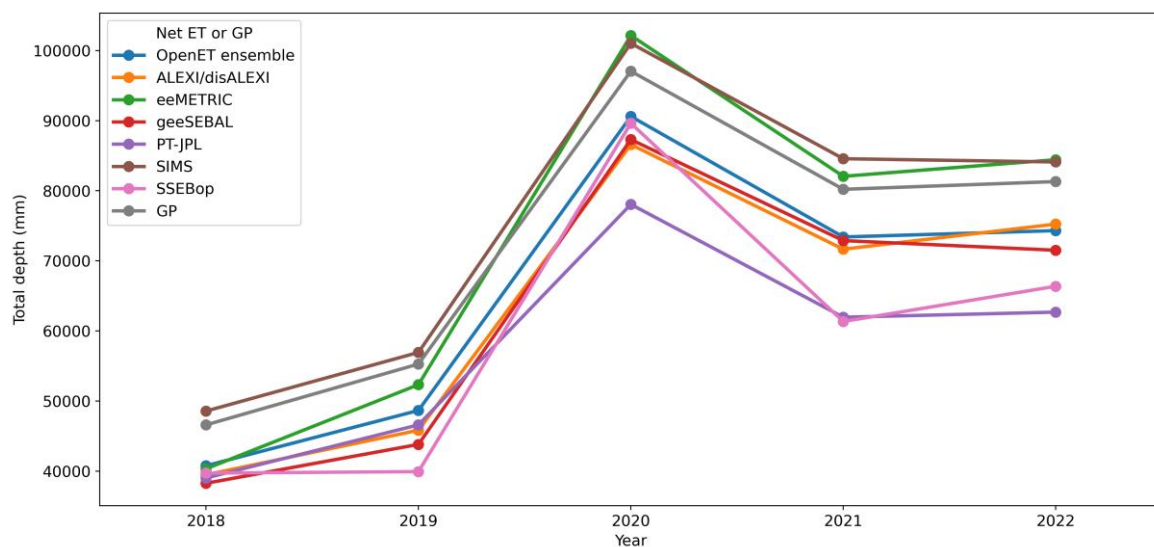
ET Model	<i>GP</i> depth metrics				Slope
	R^2	RMSE (%)	MAE (%)	CV (%)	
OpenET ensemble	0.6	15.33	12.11	20.44	1.1
ALEXI/DisALEXI	0.44	18.15	14.8	24.29	1.11
eeMETRIC	0.55	16.3	12.78	22.58	0.99
geeSEBAL	0.49	17.27	13.62	22.21	1.19
PT-JPL	0.51	16.99	13.16	17.47	1.25
SIMS	0.36	19.34	13.61	21.15	0.95
SSEBop	0.4	18.76	14.78	27.61	1.18

Essentially, we check the performance of these ET models over the same 533 samples as in Section 4.1. Although selecting the outliers based on the individual ET model-specific *GP/Net ET* ratios and tweaking the intervals from histogram and boxplot analyses would

have improved the corresponding metrics, using the same OpenET ensemble-derived $GP/Net\ ET$ ratios make the comparison more consistent. Table 3 shows that eeMETRIC and PT-JPL are the best ET models after the OpenET ensemble, with SIMS having the worst performance. Moreover, the slopes for eeMETRIC and SIMS are close to 1, implying that the consumptive groundwater use equals pumping, i.e., $Net\ ET = GP$, which is not practical and could be due to both these ET models being biased high (Huntington et al., 2018).



(a)



(b)

Figure 13. Comparisons of the (a) total annual ET depths and (b) total $Net\ ET$ and total reported metered GP depths for each ET model in DV, Nevada.

To investigate this issue, we compare the total annual actual ET depths (Figure 13 (a)) and the total annual *Net ET* depths with the total reported annual *GP* depths for each ET model (Figure 13 (b)). We observe that eeMETRIC is biased high between 2020 and 2022, whereas SIMS is biased high across all years. SSEBop and PT-JPL vary substantially but the *Net ET* obtained from these two models is always lower than the *GP* like in the case of ALEXI/DisALEXI, geeSEBAL, and the OpenET ensemble.

Moreover, from Table 4, and Supplementary Figures 4 and 5, we observe that the OpenET ensemble is also consistent in HB, Oregon, with similar *GP* depth R^2 , RMSE, and MAE metrics like the ones based on the SSEBop *Net ET* (which performs slightly better), and leads to the best *GP* depth precision in terms of CV. Thus, relying on the OpenET ensemble leads to a more consistent approach because of these high and low bias issues with the individual models.

Table 4. Comparison of the linear regression model metrics (*GP* depths, HB, Oregon) and slopes for different field-scale ET models used to calculate the *Net ET*. The metrics and slopes are rounded to two decimal places.

ET Model	GP depth metrics				Slope
	R^2	RMSE (%)	MAE (%)	CV (%)	
OpenET ensemble	0.46	13.56	11.09	13.41	1.2
ALEXI/DisALEXI	0.11	17.3	14.38	15.08	1.3
eeMETRIC	0.33	15.06	12.14	15.16	1.19
geeSEBAL	0.17	16.78	13.83	16.68	1.11
PT-JPL	0.3	15.38	12.46	14.19	1.32
SIMS	-1.6	29.64	16.37	30.78	1.07
SSEBop	0.48	13.31	10.56	17.92	1.23

4.4.2 ET comparison through Machine Learning

To compare the ML model performances corresponding to each ET model in DV, Nevada, we do not use the full 28 predictors like before in Section 4.3. Instead, we choose the ET model-specific *Net ET* and the actual ET and remove other ET predictors in each case. Hence, the ML models in Table 5 rely on 22 predictors (more details in Supplementary Table 2). The training, validation, and test data are generated in the same way as in Section 4.3., i.e., 70%-30% training and test data split, followed by the automatic validation data generation (20% from the training data) using the five-fold cross-validation technique.

Table 5. Comparison of the ML model metrics (*GP* depths, DV, Nevada) for different field-scale ET models used to calculate the *Net ET*. For each of the ET models, the metrics (rounded to two decimal places) are only reported for the test data obtained using the best ML model in terms of the RMSE and overfitting.

ET Model	Best ML model	<i>GP</i> depth metrics			
		R^2	RMSE (%)	MAE (%)	CV (%)
OpenET ensemble	ERT	0.62	14.96	11.47	17.06
ALEXI/DisALEXI	RF	0.59	15.62	12.23	15.93
eeMETRIC	RF	0.62	15.06	11.6	17.96
geeSEBAL	GBT	0.61	15.16	11.92	17.92
PT-JPL	GBT	0.61	15.25	11.65	18.53
SIMS	GBT	0.6	15.39	11.82	18.61
SSEBop	ERT	0.59	15.52	12.13	16.43

From Table 5, we find that the OpenET ensemble leads to the best performance metrics in terms of R^2 , RMSE, and MAE. Although the ML models appear to be more robust to changes in the ET models compared to the linear regression, these results are only for a single test data. Ideally, these comparisons should be repeated over thousands of model iterations

and train-test partitions for more reliable reporting of these metrics. Nevertheless, the OpenET ensemble product demonstrates consistent results across different statistical and ML modeling paradigms and the two study areas (DV, Nevada and HB, Oregon).

5. CONCLUSIONS

This is the first study to predict field-scale groundwater pumping and concurrently provide estimates of irrigation efficiencies using integrated remote sensing, irrigation, and climate data in a statistical learning framework. Here, we employed statistical (linear regression and bootstrapping) and ensemble machine learning (Random Forests, Gradient Boosting Trees, and Extremely Randomized Trees) approaches to predict field-scale groundwater pumping in Diamond Valley, Nevada, and Harney Basin, Oregon. We relied on several remote sensing, irrigation, and climate datasets for modeling. The primary datasets include OpenET (Melton et al., 2021) ensemble-derived field-scale actual evapotranspiration, ET-Demands (USBR, 2023) and gridMET (Abatzoglou, 2013)-derived effective precipitation, and carefully attributed field boundaries and water source type data (Huntington et al., 2018; Beamer & Hoskinson, 2021). Moreover, we ingested multiple temporally static (elevation, soil depth, saturated hydraulic conductivity, hydrologic soil group) and dynamic geospatial datasets (reference evapotranspiration, relative humidity, air temperature, NDVI, and others) as additional predictors to the machine learning models.

The linear regression and machine learning model results demonstrate that the OpenET ensemble product leads to more consistent results compared to the individual ET models across the two study areas and simultaneously aids in quality assurance and quality control of the reported pumping data. More specifically, the mean absolute errors for field-scale groundwater pumping depth are 12% and 11% for DV and HB, respectively, and the corresponding root mean square errors are 15% and 14%. The regression models can explain

675 50%-60% variance in the pumping depths and ~90% variance in the pumping volumes.
676 Furthermore, the estimated average irrigation efficiency of 88% (92% and 83% for Diamond
677 Valley and Harney Basin, respectively) aligns with known center pivot system efficiencies
678 (Howell, 2002).

679 Regarding the limitations of our approach, the primary bottleneck is the amount of pre-
680 processing time involved in linking the points of diversions (wells) to the places of use
681 (fields). Matching the wells to the fields is an extremely tedious yet critical task as it directly
682 influences the model performance. Other limitations include data scarcity in both the study
683 areas, particularly the Harney Basin, where there is mixed water use, i.e., fields with both
684 groundwater and surface water rights, and hence, a few fields had to be discarded directly
685 because of this issue.

686 Still, our data-driven approach provides a more systematic way of estimating groundwater
687 pumping than conventional methods based on water right duties, potential crop ET, low-
688 quality meter readings, or assumed values. As part of future work, we aim to incorporate
689 climate model projection data to generate hindcasts and future projections of groundwater
690 pumping at regional or basin scales. The broader goal of our study is to present water
691 resource and user communities with valuable insights into water use and budgets, supporting
692 the implementation of field-scale management strategies across both metered and unmetered
693 groundwater basins in Nevada, Oregon, and other states in the western U.S. Essentially, this
694 work is an advancement toward improved field-scale evaluations of groundwater pumping,
695 consumptive groundwater use, and irrigation efficiencies, thereby contributing to more
696 efficient and sustainable water management solutions.

CRediT AUTHORSHIP CONTRIBUTION STATEMENT

Thomas J. Ott*: Conceptualization, Methodology, Software, Validation, Formal analysis, Investigation, Data Curation, Visualization, Writing – Original Draft; **Sayantana Majumdar***: Conceptualization, Methodology, Software, Investigation, Formal analysis, Validation, Visualization, Writing – Original Draft, Writing – Review & Editing; **Justin L. Huntington**: Funding acquisition, Supervision, Project administration, Conceptualization, Methodology, Investigation, Writing – Review & Editing; **Christopher Pearson**: Data Curation; **Matt Bromley**: Data Curation; **Blake A. Minor**: Data Curation; **Charles G. Morton**: Data Curation; **Sachiko Sueki**: Data Curation; **Jordan P. Beamer**: Data Curation, Visualization; **Richard Jasoni**: Supervision.

*These two authors have contributed equally.

ACKNOWLEDGMENTS

We would like to express our gratitude for the support received from the State of Nevada / U.S. Department of Treasury project number 27042. Our appreciation extends to the open-source software and data communities for their generosity in making their resources available to the public. We also acknowledge the invaluable contribution of the Nevada Division of Water Resources and the Oregon Water Resources Department for providing the necessary datasets pertaining to groundwater pumping, places of use, and other shapefiles used in this research. We also extend our gratitude to Dr. Richard G. Niswonger (U.S. Geological Survey) for his helpful suggestions on handling discrepancies in the metered pumping data. Furthermore, we are thankful to our colleagues and families for their unwavering motivation and support throughout this endeavor. It is important to note that any opinions, findings, conclusions, or recommendations presented in this manuscript are solely those of the authors and do not necessarily reflect the viewpoints of the funding agencies.

DATA AVAILABILITY

The project codes, pumping, and irrigation data are publicly available at <https://github.com/montimaj/OpenET-GW>. All the remote sensing and climate data are publicly available and were automatically downloaded using the Google Earth Engine Python API.

DECLARATION OF COMPETING INTEREST

The authors declare that they have no known competing financial interests or personal relationships that could have appeared to influence the work reported in this paper.

REFERENCES

- Abatzoglou, J. T. (2013). Development of gridded surface meteorological data for ecological applications and modelling. *International Journal of Climatology*, 33(1), 121–131. <https://doi.org/10.1002/joc.3413>
- ADWR. (2018). *Groundwater Flow Model of the Willcox Basin*. Arizona Department of Water Resources. https://new.azwater.gov/sites/default/files/Willcox_Report_2018.pdf
- ADWR. (2023). *Annual Report 2022*. https://new.azwater.gov/sites/default/files/media/ANNUALREPORT_WEB_1.pdf
- Ahamed, A., Knight, R., Alam, S., Pauloo, R., & Melton, F. (2022). Assessing the utility of remote sensing data to accurately estimate changes in groundwater storage. *Science of The Total Environment*, 807, 150635. <https://doi.org/10.1016/j.scitotenv.2021.150635>
- Allen, R. G., Irmak, A., Trezza, R., Hendrickx, J. M. H., Bastiaanssen, W., & Kjaersgaard, J. (2011). Satellite-based ET estimation in agriculture using SEBAL and METRIC. *Hydrological Processes*, 25(26), 4011–4027. <https://doi.org/10.1002/hyp.8408>
- Allen, R. G., Pereira, L. S., Raes, D., & Smith, M. (1998). *Crop Evapotranspiration - Guidelines for Computing Crop Water Requirements - FAO Irrigation and drainage paper 56*. FAO - Food and Agriculture Organization of the United Nations. <http://www.fao.org/3/X0490E/x0490e00.htm>
- Allen, R. G., & Robison, C. W. (2007). *Evapotranspiration and consumptive irrigation water requirements for Idaho*. *Idaho Waters Digital Library, Digital Initiatives, University of Idaho Library*. <https://www.lib.uidaho.edu/digital/iwdl/docs/iwdl-200703.html>
- Allen, R. G., Tasumi, M., Morse, A., & Trezza, R. (2005). A Landsat-based energy balance and evapotranspiration model in Western US water rights regulation and planning. *Irrigation and Drainage Systems*, 19(3–4), 251–268. <https://doi.org/10.1007/s10795-005-5187-z>

- Allen, R. G., Tasumi, M., & Trezza, R. (2007). Satellite-Based Energy Balance for Mapping Evapotranspiration with Internalized Calibration (METRIC)—Model. *Journal of Irrigation and Drainage Engineering*, 133(4), 380–394. [https://doi.org/10.1061/\(ASCE\)0733-9437\(2007\)133:4\(380\)](https://doi.org/10.1061/(ASCE)0733-9437(2007)133:4(380))
- Anderson, M., Gao, F., Knipper, K., Hain, C., Dulaney, W., Baldocchi, D., Eichelmann, E., Hemes, K., Yang, Y., Medellin-Azuara, J., & Kustas, W. (2018). Field-Scale Assessment of Land and Water Use Change over the California Delta Using Remote Sensing. *Remote Sensing*, 10(6), 889. <https://doi.org/10.3390/rs10060889>
- Anderson, M., Norman, J. M., Mecikalski, J. R., Otkin, J. A., & Kustas, W. P. (2007). A climatological study of evapotranspiration and moisture stress across the continental United States based on thermal remote sensing: 1. Model formulation. *Journal of Geophysical Research: Atmospheres*, 112(D10). <https://doi.org/10.1029/2006JD007506>
- Bastiaanssen, W. G. M., Menenti, M., Feddes, R. A., & Holtslag, A. A. M. (1998). A remote sensing surface energy balance algorithm for land (SEBAL). 1. Formulation. *Journal of Hydrology*, 212–213, 198–212. [https://doi.org/10.1016/S0022-1694\(98\)00253-4](https://doi.org/10.1016/S0022-1694(98)00253-4)
- Beamer, J., & Hoskinson, M. (2021). *Historical Irrigation Water Use and Groundwater Pumpage Estimates in the Harney Basin, Oregon, 1991-2018 (Open File Report No. 2021-02)*. https://www.oregon.gov/owrd/wrdreports/OWRD_OFR_2021-02_Harney_Basin_METRIC_Irrigation_Use_Report.pdf
- Berger, D. L., Mayers, C. J., Garcia, C. A., Buto, S. G., & Huntington, J. M. (2016). *Budgets and chemical characterization of groundwater for the Diamond Valley flow system, central Nevada, 2011–12: U.S. Geological Survey Scientific Investigations Report 2016–5055*. <https://doi.org/10.3133/sir20165055>
- Bos, M. G., Kselik, R. A. L., Allen, R. G., & Molden, D. (2009). *Water Requirements for Irrigation and the Environment*. Springer Netherlands. <https://doi.org/10.1007/978-1-4020-8948-0>
- Breiman, L. (2001). Random Forests. *Machine Learning*, 45(1), 5–32. <https://doi.org/10.1023/A:1010933404324>
- Brookfield, A. E., Zipper, S., Kendall, A. D., Ajami, H., & Deines, J. M. (2023). Estimating Groundwater Pumping for Irrigation: A Method Comparison. *Groundwater*. <https://doi.org/10.1111/gwat.13336>
- Bugenig, D. C. (2017). *Appendix I– Groundwater Flow Modeling Report Supporting Banking Depreciation (DIAMOND VALLEY GROUNDWATER MANAGEMENT PLAN)*. <http://water.nv.gov/documents/Final%20DV%20GMP%20for%20Petition.pdf>
- Burt, C. M., Clemmens, A. J., Strelkoff, T. S., Solomon, K. H., Bliesner, R. D., Hardy, L. A., Howell, T. A., & Eisenhauer, D. E. (1997). Irrigation Performance Measures: Efficiency and Uniformity. *Journal of Irrigation and Drainage Engineering*, 123(6), 423–442. [https://doi.org/10.1061/\(ASCE\)0733-9437\(1997\)123:6\(423\)](https://doi.org/10.1061/(ASCE)0733-9437(1997)123:6(423))

- Butler, J. J., Whittemore, D. O., Wilson, B. B., & Bohling, G. C. (2018). Sustainability of aquifers supporting irrigated agriculture: a case study of the High Plains aquifer in Kansas. *Water International*, 43(6), 815–828. <https://doi.org/10.1080/02508060.2018.1515566>
- Carroll, R. W. H., Pohll, G., McGraw, D., Garner, C., Knust, A., Boyle, D., Minor, T., Bassett, S., & Pohlmann, K. (2010). Mason Valley Groundwater Model: Linking Surface Water and Groundwater in the Walker River Basin, Nevada ¹. *JAWRA Journal of the American Water Resources Association*, 46(3), 554–573. <https://doi.org/10.1111/j.1752-1688.2010.00434.x>
- Daly, C., Halbleib, M., Smith, J. I., Gibson, W. P., Doggett, M. K., Taylor, G. H., Curtis, J., & Pasteris, P. P. (2008). Physiographically sensitive mapping of climatological temperature and precipitation across the conterminous United States. *International Journal of Climatology*, 28(15), 2031–2064. <https://doi.org/10.1002/joc.1688>
- Dastane, N. G. (1974). *Effective Rainfall in Irrigated Agriculture (Volume 25 of Irrigation and drainage paper)*. Food and Agriculture Organization of the United Nations. <https://www.fao.org/3/X5560E/X5560E00.htm>
- Deines, J. M., Kendall, A. D., Butler, J. J., & Hyndman, D. W. (2019). Quantifying irrigation adaptation strategies in response to stakeholder-driven groundwater management in the US High Plains Aquifer. *Environmental Research Letters*, 14(4), 044014. <https://doi.org/10.1088/1748-9326/aafe39>
- Dieter, C. A., Maupin, M. A., Caldwell, R. R., Harris, M. A., Ivahnenko, T. I., Lovelace, J. K., Barber, N. L., & Linsey, K. S. (2018). *Estimated use of water in the United States in 2015: U.S. Geological Survey Circular 1441*. <https://doi.org/10.3133/cir1441>
- Dogrul, E. C., Brush, C., & Kadir, T. (2016). Groundwater Modeling in Support of Water Resources Management and Planning under Complex Climate, Regulatory, and Economic Stresses. *Water*, 8(12), 592. <https://doi.org/10.3390/w8120592>
- Fanning, J. L., Schwarz, G. E., & Lewis, W. C. (2001). *A field and statistical modeling study to estimate irrigation water use at Benchmark Farms study sites in southwestern Georgia, 1995-96 (U.S. Geological Survey Water-Resources Investigations Report 2000-4292)*. <https://doi.org/10.3133/wri20004292>
- Faunt, C. C. (2009). Groundwater availability of the Central Valley Aquifer, California. In C. C. Faunt (Ed.), *U.S. Geological Survey Professional Paper 1766*. <https://doi.org/10.3133/pp1766>
- Feddes, R. A., Kabat, P., Van Bakel, P. J. T., Bronswijk, J. J. B., & Halbertsma, J. (1988). Modelling soil water dynamics in the unsaturated zone — State of the art. *Journal of Hydrology*, 100(1–3), 69–111. [https://doi.org/10.1016/0022-1694\(88\)90182-5](https://doi.org/10.1016/0022-1694(88)90182-5)
- Filippelli, S. K., Sloggy, M. R., Vogeler, J. C., Manning, D. T., Goemans, C., & Senay, G. B. (2022). Remote sensing of field-scale irrigation withdrawals in the central Ogallala aquifer region. *Agricultural Water Management*, 271, 107764. <https://doi.org/10.1016/j.agwat.2022.107764>

- Fisher, J. B., Tu, K. P., & Baldocchi, D. D. (2008). Global estimates of the land–atmosphere water flux based on monthly AVHRR and ISLSCP-II data, validated at 16 FLUXNET sites. *Remote Sensing of Environment*, 112(3), 901–919. <https://doi.org/10.1016/j.rse.2007.06.025>
- Foster, T., Mieno, T., & Brozović, N. (2020). Satellite-Based Monitoring of Irrigation Water Use: Assessing Measurement Errors and Their Implications for Agricultural Water Management Policy. *Water Resources Research*, 56(11). <https://doi.org/10.1029/2020WR028378>
- Frenzel, S. A. (1985). Comparison of Methods for Estimating Ground-Water Pumpage for Irrigation. *Ground Water*, 23(2), 220–226. <https://doi.org/10.1111/j.1745-6584.1985.tb02795.x>
- Friedman, J. H. (2001). Greedy Function Approximation: A Gradient Boosting Machine. *The Annals of Statistics*, 29(5), 1189–1232. <https://jerryfriedman.su.domains/ftp/trebst.pdf>
- Garcia, C. A., Corson-Dosch, N. T., Beamer, J. P., Gingerich, S. B., Grondin, G. H., Overstreet, B. T., Haynes, J. V., & Hoskinson, M. D. (2021). *Hydrologic budget of the Harney Basin groundwater system, southeastern Oregon (ver. 1.1, November 2022): U.S. Geological Survey Scientific Investigations Report 2021–5128, 144 p.* <https://doi.org/10.3133/sir20215128>
- Geurts, P., Ernst, D., & Wehenkel, L. (2006). Extremely randomized trees. *Machine Learning*, 63(1), 3–42. <https://doi.org/10.1007/s10994-006-6226-1>
- Gingerich, S. B., Garcia, C. A., & Johnson, H. M. (2022). *Groundwater resources of the Harney Basin, southeastern Oregon: U.S. Geological Survey Fact Sheet.* <https://doi.org/10.3133/fs20223052>
- Gingerich, S. B., Johnson, H. M., Boschmann, D. E., Grondin, G. H., & Garcia, C. A. (2022). *Groundwater resources of the Harney Basin, Oregon: U.S. Geological Survey Scientific Investigations Report 2021–5103, 118 p.* <https://doi.org/10.3133/sir20215103>
- Gorelick, N., Hancher, M., Dixon, M., Ilyushchenko, S., Thau, D., & Moore, R. (2017). Google Earth Engine: Planetary-scale geospatial analysis for everyone. *Remote Sensing of Environment*, 202, 18–27. <https://doi.org/10.1016/j.rse.2017.06.031>
- Hasan, M. F., Smith, R., Vajedian, S., Pommerenke, R., & Majumdar, S. (2023). Global land subsidence mapping reveals widespread loss of aquifer storage capacity. *Nature Communications*, 14(1), 6180. <https://doi.org/10.1038/s41467-023-41933-z>
- Hastie, T., Tibshirani, R., & Friedman, J. (2001). *The Elements of Statistical Learning: Data Mining, Inference, and Prediction*. Springer New York.
- Hawkins, R. H., Hjelmfelt, A. T., & Zevenbergen, A. W. (1985). Runoff Probability, Storm Depth, and Curve Numbers. *Journal of Irrigation and Drainage Engineering*, 111(4), 330–340. [https://doi.org/10.1061/\(ASCE\)0733-9437\(1985\)111:4\(330\)](https://doi.org/10.1061/(ASCE)0733-9437(1985)111:4(330))

- Herrera-García, G., Ezquerro, P., Tomás, R., Béjar-Pizarro, M., López-Vinielles, J., Rossi, M., Mateos, R. M., Carreón-Freyre, D., Lambert, J., Teatini, P., Cabral-Cano, E., Erkens, G., Galloway, D., Hung, W.-C., Kakar, N., Sneed, M., Tosi, L., Wang, H., & Ye, S. (2021). Mapping the global threat of land subsidence. *Science*, 371(6524), 34 LP – 36. <https://doi.org/10.1126/science.abb8549>
- Howell, T. (2002). Irrigation Efficiency. In R. Lal (Ed.), *Encyclopedia of Soil Science* (1st ed.). Marcel Dekker, Inc. https://www.researchgate.net/publication/43256707_Irrigation_Efficiency
- Huntington, J., & Allen, R. G. (2009). Evapotranspiration and Net Irrigation Water Requirements for Nevada. *World Environmental and Water Resources Congress 2009*, 1–15. [https://doi.org/10.1061/41036\(342\)420](https://doi.org/10.1061/41036(342)420)
- Huntington, J., Bromley, M., Morton, C. G., & Minor, T. (2018). *Remote Sensing Estimates of Evapotranspiration from Irrigated Agriculture, Northwestern Nevada and Northeastern California (DRI Publication No. 41275 prepared for the U.S. Bureau of Reclamation)*. https://s3-us-west-2.amazonaws.com/webfiles.dri.edu/Huntington/Huntington_et_al_2018_-_DRI_41275.pdf
- Huntington, J., Gangopadhyay, S., Spears, M., Allen, R. G., King, D., Morton, C., Harrison, A., McEvoy, D., Joros, A., & Pruitt, T. (2015). *West-Wide Climate Risk Assessments: Irrigation Demand and Reservoir Evaporation Projections (Technical Memorandum No. 68-68210-2014-01)* (U.S. Bureau of Reclamation, Ed.). U.S. Bureau of Reclamation. <https://www.usbr.gov/watersmart/baseline/docs/irrigationdemand/irrigationdemands.pdf>
- Huntington, J., Pearson, C., Minor, B., Volk, J., Morton, C., Melton, F., & Allen, R. (2022). *Upper Colorado River Basin OpenET Intercomparison Summary: Prepared for U.S. Bureau of Reclamation*. <https://doi.org/10.13140/RG.2.2.21605.88808>
- Hurr, R. T., & Litke, D. W. (1989). *Estimating pumping time and ground-water withdrawals using energy- consumption data (U.S. Geological Survey Water-Resources Investigations Report 89-4107)*. <https://doi.org/10.3133/wri894107>
- Jordahl, K., Bossche, J. Van den, Fleischmann, M., Wasserman, J., McBride, J., Gerard, J., Tratner, J., Perry, M., Badaracco, A. G., Farmer, C., Hjelle, G. A., Snow, A. D., Cochran, M., Gillies, S., Culbertson, L., Bartos, M., Eubank, N., maxalbert, Bilogur, A., ... Leblanc, F. (2020). *geopandas/geopandas: v0.8.1 (v0.8.1)*. Zenodo. <https://doi.org/10.5281/ZENODO.3946761>
- Ke, G., Meng, Q., Finley, T., Wang, T., Chen, W., Ma, W., Ye, Q., & Liu, T.-Y. (2017). LightGBM: A Highly Efficient Gradient Boosting Decision Tree. In I. Guyon, U. V Luxburg, S. Bengio, H. Wallach, R. Fergus, S. Vishwanathan, & R. Garnett (Eds.), *Advances in Neural Information Processing Systems* (Vol. 30). Curran Associates, Inc. <https://proceedings.neurips.cc/paper/2017/file/6449f44a102fde848669bdd9eb6b76fa-Paper.pdf>

911 Kumar, R., Kumar, M., Farooq, Z., & Dadhich, S. M. (2017). Evaluation of models and
 912 approaches for effective rainfall in irrigated agriculture - An overview. *Journal of Soil*
 913 *and Water Conservation*, 16(1), 32. <https://doi.org/10.5958/2455-7145.2017.00012.1>

914 Laipelt, L., Henrique Bloedow Kayser, R., Santos Fleischmann, A., Ruhoff, A., Bastiaanssen,
 915 W., Erickson, T. A., & Melton, F. (2021). Long-term monitoring of evapotranspiration
 916 using the SEBAL algorithm and Google Earth Engine cloud computing. *ISPRS Journal*
 917 *of Photogrammetry and Remote Sensing*, 178, 81–96.
 918 <https://doi.org/10.1016/j.isprsjprs.2021.05.018>

919 Lamb, S. E., Haacker, E. M. K., & Smidt, S. J. (2021). Influence of Irrigation Drivers Using
 920 Boosted Regression Trees: Kansas High Plains. *Water Resources Research*, 57(5).
 921 <https://doi.org/10.1029/2020WR028867>

922 Levy, Z. F., Jurgens, B. C., Burow, K. R., Voss, S. A., Faulkner, K. E., Arroyo-Lopez, J. A.,
 923 & Fram, M. S. (2021). Critical Aquifer Overdraft Accelerates Degradation of
 924 Groundwater Quality in California’s Central Valley During Drought. *Geophysical*
 925 *Research Letters*, 48(17). <https://doi.org/10.1029/2021GL094398>

926 Little, K. E., Hayashi, M., & Liang, S. (2016). Community-Based Groundwater Monitoring
 927 Network Using a Citizen-Science Approach. *Groundwater*, 54(3), 317–324.
 928 <https://doi.org/10.1111/gwat.12336>

929 Majumdar, S., Smith, R., Butler, J. J., & Lakshmi, V. (2020). Groundwater withdrawal
 930 prediction using integrated multitemporal remote sensing data sets and machine
 931 learning. *Water Resources Research*, 56(11), e2020WR028059.
 932 <https://doi.org/10.1029/2020WR028059>

933 Majumdar, S., Smith, R., Conway, B. D., Butler, J. J., Lakshmi, V., & Dagli, C. H. (2021).
 934 Estimating Local-Scale Groundwater Withdrawals Using Integrated Remote Sensing
 935 Products and Deep Learning. *2021 IEEE International Geoscience and Remote Sensing*
 936 *Symposium IGARSS*, 4304–4307. <https://doi.org/10.1109/IGARSS47720.2021.9554784>

937 Majumdar, S., Smith, R., Conway, B. D., & Lakshmi, V. (2022). Advancing Remote Sensing
 938 and Machine Learning-Driven Frameworks for Groundwater Withdrawal Estimation in
 939 Arizona: Linking Land Subsidence to Groundwater Withdrawals. *Hydrological*
 940 *Processes*, 36(11), e14757. <https://doi.org/10.1002/hyp.14757>

941 Martin, D. J., Regan, R. S., Haynes, J. V., Read, A. L., Henson, W. R., Stewart, J. S., Brandt,
 942 J. T., & Niswonger, R. G. (2023). *Irrigation water use reanalysis for the 2000-20 period*
 943 *by HUC12, month, and year for the conterminous United States: U.S. Geological Survey*
 944 *data release*. <https://doi.org/10.5066/P9YWR00J>

945 Mefford, B., & Prairie, J. (2022). *Assessing Agricultural Consumptive Use in the Upper*
 946 *Colorado River Basin - Phase III Report. U.S. Bureau of Reclamation and the Upper*
 947 *Colorado River Commission*. <http://www.ucrcommission.com/reports-studies/>

948 Megdal, S. B., Gerlak, A. K., Varady, R. G., & Huang, L.-Y. (2015). Groundwater
 949 Governance in the United States: Common Priorities and Challenges. *Groundwater*,
 950 53(5), 677–684. <https://doi.org/10.1111/gwat.12294>

951 Melton, F., Huntington, J., Grimm, R., Herring, J., Hall, M., Rollison, D., Erickson, T., Allen,
 952 R., Anderson, M., Fisher, J. B., Kilic, A., Senay, G. B., Volk, J., Hain, C., Johnson, L.,
 953 Ruhoff, A., Blankenau, P., Bromley, M., Carrara, W., ... Anderson, R. G. (2021).
 954 OpenET: Filling a Critical Data Gap in Water Management for the Western United
 955 States. *JAWRA Journal of the American Water Resources Association*.
 956 <https://doi.org/10.1111/1752-1688.12956>

957 Melton, F., Johnson, L. F., Lund, C. P., Pierce, L. L., Michaelis, A. R., Hiatt, S. H., Guzman,
 958 A., Adhikari, D. D., Purdy, A. J., Rosevelt, C., Votava, P., Trout, T. J., Temesgen, B.,
 959 Frame, K., Sheffner, E. J., & Nemani, R. R. (2012). Satellite Irrigation Management
 960 Support With the Terrestrial Observation and Prediction System: A Framework for
 961 Integration of Satellite and Surface Observations to Support Improvements in
 962 Agricultural Water Resource Management. *IEEE Journal of Selected Topics in Applied*
 963 *Earth Observations and Remote Sensing*, 5(6), 1709–1721.
 964 <https://doi.org/10.1109/JSTARS.2012.2214474>

965 Meza, I., Siebert, S., Döll, P., Kusche, J., Herbert, C., Eyshi Rezaei, E., Nouri, H., Gerdener,
 966 H., Popat, E., Frischen, J., Naumann, G., Vogt, J. V., Walz, Y., Sebesvari, Z., &
 967 Hagenlocher, M. (2020). Global-scale drought risk assessment for agricultural systems.
 968 *Natural Hazards and Earth System Sciences*, 20(2), 695–712.
 969 <https://doi.org/10.5194/nhess-20-695-2020>

970 NASA JPL (2020). *NASADEM Merged DEM Global 1 arc second V001 [Data set]*. NASA
 971 EOSDIS Land Processes Distributed Active Archive Center.
 972 https://doi.org/10.5067/MEASURES/NASADEM/NASADEM_HGT.001

973 NDWR. (1985). *AMARGOSA VALLEY BASIN #230 1985 GROUNDWATER PUMPAGE*
 974 *INVENTORY*. [http://water.nv.gov/Pumpage%20Inventories/230%20-](http://water.nv.gov/Pumpage%20Inventories/230%20-%20Amargosa%20Valley/230%20-%201985%20-%20Amargosa%20Valley.pdf)
 975 [%20Amargosa%20Valley/230%20-%201985%20-%20Amargosa%20Valley.pdf](http://water.nv.gov/Pumpage%20Inventories/230%20-%20Amargosa%20Valley/230%20-%201985%20-%20Amargosa%20Valley.pdf)

976 NDWR. (2020). *Diamond Valley Groundwater Management Plan*.
 977 [http://water.nv.gov/Diamond%20Valley%20GMP/Diamond%20Valley%20GMP/Diamo](http://water.nv.gov/Diamond%20Valley%20GMP/Diamond%20Valley%20GMP/Diamond%20Valley%20GMP--Final.pdf)
 978 [nd%20Valley%20GMP--Final.pdf](http://water.nv.gov/Diamond%20Valley%20GMP/Diamond%20Valley%20GMP--Final.pdf)

979 NDWR. (2021). *GROUNDWATER APPROPRIATIONS & COMMITMENTS*.
 980 [https://www.leg.state.nv.us/App/NELIS/REL/82nd2023/ExhibitDocument/OpenExhibit](https://www.leg.state.nv.us/App/NELIS/REL/82nd2023/ExhibitDocument/OpenExhibitDocument?exhibitId=66244&fileDownloadName=DivisionofWaterResourcesAnswerstoCommitteeQuestions.pdf)
 981 [Document?exhibitId=66244&fileDownloadName=DivisionofWaterResourcesAnswerst](https://www.leg.state.nv.us/App/NELIS/REL/82nd2023/ExhibitDocument/OpenExhibitDocument?exhibitId=66244&fileDownloadName=DivisionofWaterResourcesAnswerstoCommitteeQuestions.pdf)
 982 [oCommitteeQuestions.pdf](https://www.leg.state.nv.us/App/NELIS/REL/82nd2023/ExhibitDocument/OpenExhibitDocument?exhibitId=66244&fileDownloadName=DivisionofWaterResourcesAnswerstoCommitteeQuestions.pdf)

983 NDWR. (2022). *AMARGOSA DESERT HYDROGRAPHIC BASIN 14-230 GROUNDWATER*
 984 *PUMPAGE INVENTORY, WATER YEAR 2021*.
 985 [http://water.nv.gov/Pumpage%20Inventories/230%20-](http://water.nv.gov/Pumpage%20Inventories/230%20-%20Amargosa%20Valley/230%20-%202021%20-%20Amargosa%20Valley.pdf)
 986 [%20Amargosa%20Valley/230%20-%202021%20-%20Amargosa%20Valley.pdf](http://water.nv.gov/Pumpage%20Inventories/230%20-%20Amargosa%20Valley/230%20-%202021%20-%20Amargosa%20Valley.pdf)

987 OpenET. (2023). *OpenET Methodologies*. <https://openetdata.org/methodologies/>

988 Owen, D., Cantor, A., Nylen, N. G., Harter, T., & Kiparsky, M. (2019). California
 989 groundwater management, science-policy interfaces, and the legacies of artificial legal
 990 distinctions. *Environmental Research Letters*, 14(4), 045016.
 991 <https://doi.org/10.1088/1748-9326/ab0751>

992 OWRD. (2015). *Oregon Statewide Long-Term Water Demand Forecast*.
993 <http://www.oregon.gov/OWRD/>

994 Patwardhan, A. S., Nieber, J. L., & Johns, E. L. (1990). Effective Rainfall Estimation
995 Methods. *Journal of Irrigation and Drainage Engineering*, 116(2), 182–193.
996 [https://doi.org/10.1061/\(ASCE\)0733-9437\(1990\)116:2\(182\)](https://doi.org/10.1061/(ASCE)0733-9437(1990)116:2(182))

997 Pedregosa, F., Varoquaux, G., Gramfort, A., Michel, V., Thirion, B., Grisel, O., Blondel, M.,
998 Prettenhofer, P., Weiss, R., Dubourg, V., Vanderplas, J., Passos, A., Cournapeau, D.,
999 Brucher, M., Perrot, M., & Duchesnay, E. (2011). Scikit-learn: Machine Learning in
1000 Python. *Journal of Machine Learning Research*, 12, 2825–2830.
1001 <http://www.jmlr.org/papers/volume12/pedregosa11a/pedregosa11a.pdf>

1002 Pereira, L. S., Paredes, P., Melton, F., Johnson, L., Wang, T., López-Urrea, R., Cancela, J. J.,
1003 & Allen, R. G. (2020). Prediction of crop coefficients from fraction of ground cover and
1004 height. Background and validation using ground and remote sensing data. *Agricultural*
1005 *Water Management*, 241, 106197. <https://doi.org/10.1016/j.agwat.2020.106197>

1006 Reilly, T. E., Dennehy, K. F., Alley, W. M., & Cunningham, W. L. (2008). *Ground-water*
1007 *availability in the United States (USGS Publications Warehouse)*.
1008 <https://doi.org/10.3133/cir1323>

1009 Ruess, P. J., Konar, M., Wanders, N., & Bierkens, M. (2023). Irrigation by Crop in the
1010 Continental United States From 2008 to 2020. *Water Resources Research*, 59(2).
1011 <https://doi.org/10.1029/2022WR032804>

1012 Said, A., Stevens, D. K., & Schlke, G. (2005). ESTIMATING WATER BUDGET IN A
1013 REGIONAL AQUIFER USING HSPF-MODFLOW INTEGRATED MODEL. *Journal*
1014 *of the American Water Resources Association*, 41(1), 55–66.
1015 <https://doi.org/10.1111/j.1752-1688.2005.tb03717.x>

1016 Scanlon, B. R., Faunt, C. C., Longuevergne, L., Reedy, R. C., Alley, W. M., McGuire, V. L.,
1017 & McMahon, P. B. (2012). Groundwater depletion and sustainability of irrigation in the
1018 US High Plains and Central Valley. *Proceedings of the National Academy of Sciences*,
1019 109(24), 9320–9325. <https://doi.org/10.1073/pnas.1200311109>

1020 Schmid, W. (2004). *A farm package for MODFLOW-2000 : simulation of irrigation demand*
1021 *and conjunctively managed surface-water and ground-water supply (PhD Dissertation)*
1022 [Department of Hydrology and Water Resources, The University of Arizona].
1023 <https://repository.arizona.edu/handle/10150/191271>

1024 Senay, G. B. (2018). Satellite Psychrometric Formulation of the Operational Simplified
1025 Surface Energy Balance (SSEBop) Model for Quantifying and Mapping
1026 Evapotranspiration. *Applied Engineering in Agriculture*, 34(3), 555–566.
1027 <https://doi.org/10.13031/aea.12614>

1028 Senay, G. B., Bohms, S., Singh, R. K., Gowda, P. H., Velpuri, N. M., Alemu, H., & Verdin,
1029 J. P. (2013). Operational Evapotranspiration Mapping Using Remote Sensing and
1030 Weather Datasets: A New Parameterization for the SSEB Approach. *JAWRA Journal of*
1031 *the American Water Resources Association*, 49(3), 577–591.
1032 <https://doi.org/10.1111/jawr.12057>

1033 Senay, G. B., Friedrichs, M., Morton, C., Parrish, G. E. L., Schauer, M., Khand, K., Kagone,
 1034 S., Boiko, O., & Huntington, J. (2022). Mapping actual evapotranspiration using
 1035 Landsat for the conterminous United States: Google Earth Engine implementation and
 1036 assessment of the SSEBop model. *Remote Sensing of Environment*, 275, 113011.
 1037 <https://doi.org/10.1016/j.rse.2022.113011>

1038 Sheppard, S. A., & Terveen, L. (2011). Quality is a verb. *Proceedings of the 7th International*
 1039 *Symposium on Wikis and Open Collaboration*, 29–38.
 1040 <https://doi.org/10.1145/2038558.2038565>

1041 Smith, R., Knight, R., Chen, J., Reeves, J. A., Zebker, H. A., Farr, T., & Liu, Z. (2017).
 1042 Estimating the permanent loss of groundwater storage in the southern San Joaquin
 1043 Valley, California. *Water Resources Research*, 53(3), 2133–2148.
 1044 <https://doi.org/10.1002/2016WR019861>

1045 Smith, R., Knight, R., & Fendorf, S. (2018). Overpumping leads to California groundwater
 1046 arsenic threat. *Nature Communications*, 9(1), 2089. [https://doi.org/10.1038/s41467-018-](https://doi.org/10.1038/s41467-018-04475-3)
 1047 [04475-3](https://doi.org/10.1038/s41467-018-04475-3)

1048 Smith, R., & Li, J. (2021). Modeling elastic and inelastic pumping-induced deformation with
 1049 incomplete water level records in Parowan Valley, Utah. *Journal of Hydrology*, 601,
 1050 126654. <https://doi.org/10.1016/j.jhydrol.2021.126654>

1051 Smith, R., Li, J., Grote, K., & Butler, J. (2023). Estimating Aquifer System Storage Loss
 1052 With Water Levels, Pumping and InSAR Data in the Parowan Valley, Utah. *Water*
 1053 *Resources Research*, 59(4). <https://doi.org/10.1029/2022WR034095>

1054 Smith, R., & Majumdar, S. (2020). Groundwater storage loss associated with land subsidence
 1055 in Western United States mapped using machine learning. *Water Resources Research*,
 1056 56(7), e2019WR026621. <https://doi.org/10.1029/2019WR026621>

1057 Stamm, G. G. (1967). *Problems and Procedures in Determining Water Supply Requirements*
 1058 *for Irrigation Projects* (pp. 769–785). <https://doi.org/10.2134/agronmonogr11.c45>

1059 Thornton, P. E., Shrestha, R., Thornton, M., Kao, S.-C., Wei, Y., & Wilson, B. E. (2021).
 1060 Gridded daily weather data for North America with comprehensive uncertainty
 1061 quantification. *Scientific Data*, 8(1), 190. <https://doi.org/10.1038/s41597-021-00973-0>

1062 USBR. (2016). *Historical and Future Irrigation Water Requirements for Select Reclamation*
 1063 *Project Areas*.
 1064 [https://www.usbr.gov/watersmart/baseline/docs/historicalandfutureirrigationwaterrequir-](https://www.usbr.gov/watersmart/baseline/docs/historicalandfutureirrigationwaterrequirements.pdf)
 1065 [ements.pdf](https://www.usbr.gov/watersmart/baseline/docs/historicalandfutureirrigationwaterrequirements.pdf)

1066 USBR. (2019). *ET-Demands*. <https://github.com/usbr/et-demands>

1067 USBR. (2023). *WaterSMART Basin Study*.
 1068 https://www.usbr.gov/watersmart/bsp/docs/BasinStudy_FactSheet_2023.pdf

1069 USDA. (2023). *National Agriculture Imagery Program (NAIP)*. [https://naip-](https://naip-usdaonline.hub.arcgis.com/)
 1070 [usdaonline.hub.arcgis.com/](https://naip-usdaonline.hub.arcgis.com/)

- 1071 USDA Farm Service Agency. (2017). *Common Land Unit (CLU)*.
 1072 <https://www.fsa.usda.gov/Assets/USDA-FSA-Public/usdafiles/APFO/support->
 1073 [documents/pdfs/clu_infosheet_2017_Final.pdf](https://www.fsa.usda.gov/Assets/USDA-FSA-Public/usdafiles/APFO/support-documents/pdfs/clu_infosheet_2017_Final.pdf)
- 1074 USDA NRCS. (2004). Chapter 9 Hydrologic Soil-Cover Complexes. In *Part 630 Hydrology*
 1075 *National Engineering Handbook*.
 1076 <https://directives.sc.egov.usda.gov/OpenNonWebContent.aspx?content=17758.wba>
- 1077 USDA SCS. (1993). Chapter 2 Irrigation Water Requirements. In *Part 623 National*
 1078 *Engineering Handbook*. USDA Soil Conservation Service.
 1079 <https://www.wcc.nrcs.usda.gov/ftpref/wntsc/waterMgt/irrigation/NEH15/ch2.pdf>
- 1080 USGS. (2023). *1 Arc-second Digital Elevation Models (DEMs) - USGS National Map 3DEP*
 1081 *Downloadable Data Collection: U.S. Geological Survey*.
 1082 <https://www.sciencebase.gov/catalog/item/4f70aa71e4b058caae3f8de1>
- 1083 Van Rossum, G., & Drake, F. L. (2009). *Python 3 Reference Manual*. CreateSpace.
 1084 <https://dl.acm.org/doi/book/10.5555/1593511>
- 1085 Walkinshaw, M., O'Geen, A. T., & Beaudette, D. E. (2022). "Soil Properties." California Soil
 1086 Resource Lab. casoilresource.lawr.ucdavis.edu/soil-properties/.
- 1087 Wei, S., Xu, T., Niu, G.-Y., & Zeng, R. (2022). Estimating Irrigation Water Consumption
 1088 Using Machine Learning and Remote Sensing Data in Kansas High Plains. *Remote*
 1089 *Sensing*, 14(13), 3004. <https://doi.org/10.3390/rs14133004>
- 1090 Wilson, J. L. (2021). Aquaculture and Irrigation Water-Use Model (AIWUM) version 1.0—
 1091 An agricultural water-use model developed for the Mississippi Alluvial Plain, 1999–
 1092 2017. In *Scientific Investigations Report*. U.S. Geological Survey.
 1093 <https://doi.org/10.3133/sir20215011>
- 1094 Xia, Y., Mitchell, K., Ek, M., Sheffield, J., Cosgrove, B., Wood, E., Luo, L., Alonge, C.,
 1095 Wei, H., Meng, J., Livneh, B., Lettenmaier, D., Koren, V., Duan, Q., Mo, K., Fan, Y., &
 1096 Mocko, D. (2012). Continental-scale water and energy flux analysis and validation for
 1097 the North American Land Data Assimilation System project phase 2 (NLDAS-2): 1.
 1098 Intercomparison and application of model products. *Journal of Geophysical Research:*
 1099 *Atmospheres*, 117(D3). <https://doi.org/10.1029/2011JD016048>
- 1100 Zektser, S., Loaiciga, H. A., & Wolf, J. T. (2005). Environmental impacts of groundwater
 1101 overdraft: selected case studies in the southwestern United States. *Environmental*
 1102 *Geology*, 47(3), 396–404. <https://doi.org/10.1007/s00254-004-1164-3>

1103